

A Global View of the EDM Landscape

Skyler Degenkolb¹, Nina Elmer²,
Tanmoy Modak², Margarete Mühlleitner³, and Tilman Plehn^{2,4}

¹ Physikalisches Institut, Universität Heidelberg, Germany

² Institut für Theoretische Physik, Universität Heidelberg, Germany

³ Institute for Theoretical Physics, Karlsruhe Institute of Technology, Karlsruhe, Germany

⁴ Interdisciplinary Center for Scientific Computing (IWR), Universität Heidelberg, Germany

Abstract

Permanent electric dipole moments (EDMs) are sensitive probes of the symmetry structure of elementary particles, which in turn is closely tied to the baryon asymmetry in the universe. A meaningful interpretation framework for EDM measurements has to be based on effective quantum field theory. We interpret the measurements performed to date in terms of a hadronic-scale Lagrangian, using the SFitter global analysis framework. We find that part of this Lagrangian is constrained very well, while some of the parameters suffer from too few high-precision measurements. Theory uncertainties lead to weaker model constraints, but can be controlled within the global analysis.

Contents

1	Introduction	2
2	EDM Lagrangian	3
2.1	Weak-scale Lagrangian	3
2.2	Hadronic-scale Lagrangian	4
2.3	Matched Lagrangians for semileptonic interactions	5
3	EDM Measurements	8
3.1	Nucleons	10
3.2	Open-shell (paramagnetic) systems	11
3.3	Closed-shell (diamagnetic) systems	14
3.4	Single parameter ranges	15
4	Global analysis	17
4.1	SFitter framework	17
4.2	Well-constrained model sub-space	18
4.3	Hadronic parameters from closed-shell systems	20
4.4	Poorly constrained model parameters	21
4.5	Theory uncertainties	22
5	Outlook	25
A	Alternative parametrization: short-range nucleon EDMs	28
	References	35

1 Introduction

While the Standard Model (SM) is structurally complete, it fails to explain key observations and therefore fails to qualify as a complete theory of elementary particles. The two leading shortcomings are a missing dark matter agent and a missing explanation of the baryon asymmetry in the Universe. For the latter, the Sakharov conditions [1] tell us precisely which structures would be required: (i) C- and CP-violation, (ii) baryon number violation, and (iii) a deviation from thermal equilibrium. The first condition is especially interesting, because one can read it off the fundamental Lagrangian and build, for instance, models for electroweak baryogenesis around it [2–6]. In the SM, CP symmetry is violated through the fermion mixing among three generations and through the adjoint gluon field strength. Measurements of the neutron EDM, consistent with zero, clearly show that CP violation in QCD is too small to explain the observed baryon asymmetry [7–12]. Physics beyond the Standard Model (BSM), explaining the baryon asymmetry, should then violate CP to a greater extent and with observable consequences.

Over recent years, EDM measurements have been performed on a wide range of particles, atoms, and molecules [13–16]. None has been able to confirm a signal for CP violation. To judge their combined impact on BSM physics, we need to combine them in a consistent framework. Such a global analysis must start from a Lagrangian and express the experimental limits on all EDMs in terms of its fundamental parameters. One choice is a hadronic-scale Lagrangian, describing the interactions of nucleons, pions, and electrons at the GeV scale [13, 16–19]. Alternatively, we can combine EDM measurements at the weak scale, using an effective extension of the renormalizable SM Lagrangian [14, 19–24]. Going beyond effective field theories (EFTs), an ultimate link to the cosmological motivation requires a UV-complete extension of the SM at the weak scale, for instance leptoquark models [19], extended Higgs sectors [25–27], left-right symmetry [28], or supersymmetry [29–34]. Technically, all global analyses [35] face similar challenges which we will tackle in this paper for the hadronic-scale Lagrangian.

We perform a global EDM analysis with the SFITTER analysis tool [36–40], with its focus on the comprehensive treatment of uncertainties. Our analysis provides state-of-the-art limits on the multi-dimensional model parameter space (with no assumptions made about the underlying sources of CP violation). It also allows us to judge the impact of new or proposed measurements and to identify shortcomings in relating measurements to fundamental parameters¹, while remaining easy to repeat or adapt in response to new theoretical or experimental inputs. For this purpose it is crucial to interpret all measurements in the same fundamental physics framework and to include all uncertainties and correlations, including theory uncertainties, even though these typically lack a statistical interpretation [41].

We start by introducing a consistent hadronic-scale Lagrangian, with properly chosen Wilson coefficients for our global analysis, in Sec. 2. We then use this Lagrangian to provide predictions for the measured EDMs, as detailed in Sec. 3. We start our global analysis without theory uncertainties in Sec. 4, to understand the relations among different EDM measurements in terms of the hadronic-scale Lagrangian. To extract correlations and limits on single model parameters we employ a profile likelihood. We find that the current EDM measurements define a subspace of well-constrained model parameters and an orthogonal subspace of poorly constrained parameters with narrow correlation patterns. Adding theory uncertainties on the relations between Lagrangian parameters and observables in Sec. 4.5 degrades the interpretation in terms of fundamental physics. We emphasize that this degradation does not cut into the discovery potential of EDM measurements, as probes of fundamental symmetries of elementary particles, but it hampers their interpretation as limits in fundamental physics.

¹Only a proper fundamental physics interpretation can make full use of experimental limits.

2 EDM Lagrangian

Because new sources of CP violation are motivated by cosmology and can be related to physics beyond the SM at and above the weak scale, we start by introducing CP violation into the weak-scale Lagrangian in Sec. 2.1, relate this to the GeV-scale Lagrangian in Sec. 2.2, and use simple matching arguments to simplify this hadronic-scale Lagrangian which we use as the interpretation framework for our global analysis in Sec. 2.3. A detailed analysis of CP-violating new physics at the electroweak scale includes a renormalization group evolution from the GeV-scale to the electroweak scale and is not part of this first study. Instead, we focus here on a global analysis at the hadronic scale and the role of correlations and theory uncertainties.

2.1 Weak-scale Lagrangian

The operators generating CP violation within and beyond the SM-Lagrangian, neglecting CP violation in the neutrino sector [14], appear in the Lagrangian

$$\mathcal{L}_{\text{CPV}} = \mathcal{L}_{\text{CKM}} + \mathcal{L}_{\bar{\theta}} + \mathcal{L}_{\text{dipole}} + \mathcal{L}_{\text{Weinberg}} + \mathcal{L}_{\text{EFT}}. \quad (1)$$

The first term represents CP violation at mass dimension four, from the complex phases in the CKM matrix. The second arises from the gluon field strength, also at dimension four,

$$\mathcal{L}_{\bar{\theta}} = \frac{g_3^2}{32\pi^2} \bar{\theta} \text{Tr}(G^{\mu\nu} \tilde{G}_{\mu\nu}), \quad (2)$$

where g_3 is the strong coupling, $G^{\mu\nu}$ is the gluon field strength, $\tilde{G}^{\mu\nu} = \epsilon^{\mu\nu\lambda\sigma} G_{\lambda\sigma}/2$ is its dual, and $\bar{\theta}$ is the re-scaled CP-violating parameter in QCD. The bar notation indicates that corrections from the quark mass matrix are included. In principle $\bar{\theta}$ can also be included as a model parameter, for instance in testing a specific BSM model [28]. However, we take the view that the neutron EDM experimentally constrains $\bar{\theta}$ to have such a small value that this fine-tuning problem requires a proper explanation. This means that at present there is little to be learned from including $\bar{\theta}$ as a model parameter in our global analysis.

The other three contributions in Eq.(1) are higher-dimensional and not part of a renormalizable extension of the SM-Lagrangian. Electric dipole moments of fermions d_f^E , and chromo-electric dipole moments of quarks d_q^C , appear at mass dimension five:

$$\mathcal{L}_{\text{dipole}} = -\frac{i}{2} F^{\mu\nu} \sum_{f=q,\ell} d_f^E (\bar{f} \sigma_{\mu\nu} \gamma_5 f) - \frac{i}{2} g_3 G_{\mu\nu}^a \sum_{f=q} d_q^C (\bar{q} \sigma^{\mu\nu} \gamma_5 T^a q), \quad (3)$$

where the indices q and ℓ denote quarks and leptons of all three generations. The electromagnetic field strength is $F^{\mu\nu}$. We chose the metric convention $(1, -1)$ with $\gamma_5 = -i\gamma_0\gamma_1\gamma_2\gamma_3$. The fermion spins are $\sigma_{\mu\nu} = i[\gamma_\mu, \gamma_\nu]/2$, and T^a are the $SU(3)$ generators. The Weinberg operator is again built out of the gluon field strength and introduces the gluonic chromo-electric dipole moment d^G ,

$$\mathcal{L}_{\text{Weinberg}} = \frac{1}{3} d^G f_{abc} G_{\mu\nu}^a \tilde{G}^{b\nu\rho} G_\rho^c{}^\mu. \quad (4)$$

Additional CP-violation occurs at mass dimension six and higher, generated at a new physics scale larger than the Higgs vacuum expectation value, $\Lambda > v$,

$$\mathcal{L}_{\text{EFT}} = \sum_i \frac{C_i^{(6)}}{\Lambda^2} \mathcal{O}_i^{(6)} + \mathcal{O}(\Lambda^{-3}). \quad (5)$$

Relevant dimension-6 operators that generate EDMs include the following semileptonic and quark 4-fermion operators,

$$\begin{aligned} \mathcal{L}_{\text{EFT}} \supset & C_{\ell eqd} (\bar{L}^j e_R) (\bar{d}_R Q_j) + C_{\ell equ}^{(1)} (\bar{L}^j e_R) \epsilon_{jk} (\bar{Q}^k u_R) + C_{\ell equ}^{(3)} (\bar{L}^j \sigma_{\mu\nu} e_R) \epsilon_{jk} (\bar{Q}^k \sigma_{\mu\nu} u_R) \\ & + C_{quqd}^{(1)} (\bar{Q}^j u_R) \epsilon_{jk} (\bar{Q}^k d_R) + C_{quqd}^{(8)} (\bar{Q}^j T^a u_R) \epsilon_{jk} (\bar{Q}^k T^a d_R) + \text{h.c.} \end{aligned} \quad (6)$$

The dipole moments, the Weinberg operator, and the additional 4-fermion interactions can serve as the basis for an EDM analyses in the SMEFT framework [13, 14, 19–25, 30–32]. As always, the set of higher-dimensional SMEFT operators that turn out to be most relevant depends on the high-scale BSM model that the SMEFT represents. For instance, in supersymmetric models there are no contributions from $\mathcal{O}_{quqd}^{(8)}$ and $\mathcal{O}_{\ell equ}^{(3)}$ at tree level, and the relative size of down-type and up-type quark couplings is affected by a potentially large $\tan\beta$ enhancement.

2.2 Hadronic-scale Lagrangian

The challenge with EDMs in view of the Lagrangian of Eq.(1) is that they are measured far below the electroweak scale, where the propagating degrees of freedom are leptons, non-relativistic nucleons $N = (p, n)^T$ with average mass m_N , and pions $\vec{\pi} = (\pi^+, \pi^0, \pi^-)^T$ [13, 16, 17, 19, 30, 32]. We take the particle physics convention for strong isospin, $\tau_3 |n\rangle = -|n\rangle$

When we evolve our EFT to the experimentally relevant GeV scale, only the lepton EDMs $d_\ell^E \equiv d_\ell$ in Eq.(3) of the electroweak Lagrangian in Eq.(1) remain unchanged. While for the weak-scale Lagrangian the relation between the three charged leptons, for instance the scaling with the lepton mass, raises interesting questions, we factorize the muon and tau EDMs from the hadronic-scale Lagrangian. They can be included in the same framework, but given the systems for which experimental limits are available today, the indirect constraints on EDMs of heavy leptons are many orders of magnitude weaker than for the electron and there is little interplay among the relevant model parameters.

We split the hadronic-scale Lagrangian describing EDMs at the experimentally relevant GeV scale into

$$\mathcal{L}_{\text{had}} \supset \mathcal{L}_{N,\text{sr}} + \mathcal{L}_{\pi N} + \mathcal{L}_{eN} - \frac{i}{2} F^{\mu\nu} d_e \bar{e} \sigma_{\mu\nu} \gamma_5 e. \quad (7)$$

While the observable nucleon EDMs d_N can be included directly (as for the electron), it is also possible to separate out the "short-range" parameters d_N^{sr} by explicitly calculating pion loop contributions within chiral perturbation theory. The dipole moments of the nucleons in that case now read

$$\mathcal{L}_{N,\text{sr}} = -2\bar{N} \left[d_p^{\text{sr}} \frac{1+\tau_3}{2} + d_n^{\text{sr}} \frac{1-\tau_3}{2} \right] S_\mu N v_\nu F^{\mu\nu}, \quad (8)$$

where S_μ and v_μ are the spin and velocity of the (non-relativistic) nucleon. The isoscalar and isovector contributions then determine either d_N or d_N^{sr} , as the Lagrangian parameters for the neutron and proton EDMs: we will come back to this choice of Lagrangian parameters for the nucleon EDMs in Sec. 3.1 and App. A.

Next come the interactions of pions and nucleons,

$$\begin{aligned} \mathcal{L}_{\pi N} = & \bar{N} \left[g_\pi^{(0)} \vec{\tau} \cdot \vec{\pi} + g_\pi^{(1)} \pi^0 + g_\pi^{(2)} (3\tau_3 \pi^0 - \vec{\tau} \cdot \vec{\pi}) \right] N \\ & + C_1 (\bar{N} N) \partial_\mu (\bar{N} S^\mu \bar{N}) + C_2 (\bar{N} \vec{\tau} N) \cdot \partial_\mu (\bar{N} S^\mu \bar{N} \vec{\tau}) + \dots \end{aligned} \quad (9)$$

where τ are the internal-space Pauli matrices and we neglect, for example, interactions with more than one pion. The contribution involving $g_\pi^{(2)}$ is suppressed relative to $g_\pi^{(0,1)}$ by one order in the chiral expansion [42, 43], but can be taken into account in similar fashion. In our parameterization these interactions always contribute to nuclear EDMs, and when d_N^{sr} are chosen as model parameters they additionally contribute to nucleon EDMs through calculable pion loops [17] that appear as additional terms in $\mathcal{L}_{\pi N}$ as discussed in Sec. 3.1 below.

Naive dimensional analysis [44] suggests that short-range nucleon interactions enter only at NNLO [45] in the chiral expansion [46] and can be neglected [43]. In Eq.(9) this applies to all interactions in the second line. One caveat is that a consistent treatment of long-range effects may require additional short-distance counter terms [45] that appear as effective short-range nucleon-nucleon forces. These are not presently taken into account, and theoretical coefficients for the sensitivity of specific systems to these forces are largely unavailable at present.

Finally, the higher-dimensional operators in Eq.(6) induce effective interactions that can be organized according to their tensor structure, isospin character, and their dependence on the electron and nucleon fields and spins [16, 19]:

$$\begin{aligned} \mathcal{L}_{eN} = & -\frac{G_F}{\sqrt{2}} (\bar{e}i\gamma_5 e) \bar{N} \left(C_S^{(0)} + C_S^{(1)} \tau_3 \right) N \\ & + \frac{8G_F}{\sqrt{2}} \nu_\nu (\bar{e}\sigma^{\mu\nu} e) \bar{N} \left(C_T^{(0)} + C_T^{(1)} \tau_3 \right) S_\mu N \\ & - \frac{G_F}{\sqrt{2}} (\bar{e}e) \frac{\partial^\mu}{m_N} \left[\bar{N} \left(C_P^{(0)} + C_P^{(1)} \tau_3 \right) S_\mu N \right]. \end{aligned} \quad (10)$$

In a heavy baryon expansion, the last line can be dropped at leading order [14]. However, we retain all three terms since (1) a pion pole enhancement of the isovector contribution somewhat offsets this hierarchy and (2) contributions of heavy quarks can also render it relevant for some new physics models. At this stage, the independent Lagrangian parameters for our global EDM analysis at the hadronic scale are

$$\left\{ d_e, C_S^{(0)}, C_S^{(1)}, C_T^{(0)}, C_T^{(1)}, C_P^{(0)}, C_P^{(1)}, g_\pi^{(0)}, g_\pi^{(1)}, d_n, d_p \right\}, \quad (11)$$

where the observable $d_{n,p}$ can be replaced by the short-range nucleon EDMs $d_{n,p}^{\text{sr}}$ for an alternate parameterization, as described in the Appendix.

2.3 Matched Lagrangians for semileptonic interactions

The set of model parameters defined in Eq.(11) can be further simplified by matching the semileptonic part of the hadronic-scale Lagrangian Eq.(10) to the corresponding weak-scale 4-fermion interactions of Eq.(6), both evaluated for external nucleons. The light quark content

in the nucleons is related to the nucleon Lagrangian as

$$\begin{aligned}
g_S^{(0)} \bar{\psi}_N \psi_N &= \frac{1}{2} \langle N | \bar{u}u + \bar{d}d | N \rangle \\
g_S^{(1)} \bar{\psi}_N \tau_3 \psi_N &= \frac{1}{2} \langle N | \bar{u}u - \bar{d}d | N \rangle \\
g_T^{(0)} \bar{\psi}_N \sigma_{\mu\nu} \psi_N &= \frac{1}{2} \langle N | \bar{u} \sigma_{\mu\nu} u + \bar{d} \sigma_{\mu\nu} d | N \rangle \\
g_T^{(1)} \bar{\psi}_N \sigma_{\mu\nu} \tau_3 \psi_N &= \frac{1}{2} \langle N | \bar{u} \sigma_{\mu\nu} u - \bar{d} \sigma_{\mu\nu} d | N \rangle \\
g_P^{(0)} \bar{\psi}_N \gamma_5 \psi_N &= \frac{1}{2} \langle N | \bar{u} \gamma_5 u + \bar{d} \gamma_5 d | N \rangle \\
g_P^{(1)} \bar{\psi}_N \gamma_5 \tau_3 \psi_N &= \frac{1}{2} \langle N | \bar{u} \gamma_5 u - \bar{d} \gamma_5 d | N \rangle,
\end{aligned} \tag{12}$$

which relations define the scalar, tensor, and pseudoscalar nucleon form factors $g_{S,T,P}^{(0,1)}$. Using these, the hadronic-scale Wilson coefficients in Eq.(10) can be matched to the SMEFT Wilson coefficients in Eq.(6) as [14, 16],

$$\begin{aligned}
C_S^{(0)} &= -g_S^{(0)} \frac{v^2}{\Lambda^2} \text{Im}(C_{\ell edq} - C_{\ell equ}^{(1)}) & C_S^{(1)} &= g_S^{(1)} \frac{v^2}{\Lambda^2} \text{Im}(C_{\ell edq} + C_{\ell equ}^{(1)}) \\
C_T^{(0)} &= -g_T^{(0)} \frac{v^2}{\Lambda^2} \text{Im}(C_{\ell equ}^{(3)}) & C_T^{(1)} &= -g_T^{(1)} \frac{v^2}{\Lambda^2} \text{Im}(C_{\ell equ}^{(3)}) \\
C_P^{(0)} &= g_P^{(0)} \frac{v^2}{\Lambda^2} \text{Im}(C_{\ell edq} + C_{\ell equ}^{(1)}) & C_P^{(1)} &= -g_P^{(1)} \frac{v^2}{\Lambda^2} \text{Im}(C_{\ell edq} - C_{\ell equ}^{(1)}).
\end{aligned} \tag{13}$$

Here the six couplings $C_{S,T,P}^{(0,1)}$ are expressed in terms of only three SMEFT Wilson coefficients, implying

$$\frac{C_P^{(0)}}{g_P^{(0)}} = \frac{C_S^{(1)}}{g_S^{(1)}} \quad \frac{C_T^{(0)}}{g_T^{(0)}} = \frac{C_T^{(1)}}{g_T^{(1)}} \quad \frac{C_S^{(0)}}{g_S^{(0)}} = \frac{C_P^{(1)}}{g_P^{(1)}}. \tag{14}$$

Only three independent semileptonic parameters actually enter the hadronic-scale global analysis. We choose them as $C_{S,T,P}^{(0)}$ and combine them using the known ratios of hadronic matrix elements to construct the full Lagrangian. In addition to the light quarks described by Eq.(13), the relations in Eq.(14) also must include the contributions of heavy quarks. These contributions are contained in the nucleon form factors, renormalized at an appropriate mass scale and accounting for the corresponding anomaly relations.

Note that in this way our global analysis preserves the full dependence on $C_{S,T,P}^{(0,1)}$, although only $C_{S,T,P}^{(0)}$ appear as model parameters. This remains the case regardless of isospin-violating effects, and also when including several experimental systems for which the coefficients of $C_S^{(1)}$ differ significantly, as discussed below.

The implementation of Eq.(13) for $C_S^{(0,1)}$ is particularly straightforward, because for each experimental system the effective parameter that combines the isoscalar and isovector terms is independent of the nuclear spin,

$$\begin{aligned}
C_S &= C_S^{(0)} + \frac{Z-N}{Z+N} C_S^{(1)} \\
&= C_S^{(0)} + \frac{Z-N}{Z+N} \frac{g_S^{(1)}}{g_P^{(0)}} C_P^{(0)} \quad \text{with} \quad \frac{g_S^{(1)}}{g_P^{(0)}} \approx 0.1.
\end{aligned} \tag{15}$$

In the second step we replace $C_S^{(1)}$ with $C_P^{(0)}$, reflecting Eq.(13). Since $g_S^{(1)}$ is already suppressed relative to $g_S^{(0)}$ by the small isospin violation of the nucleon matrix element, one could argue that $C_S^{(1)} \ll C_S^{(0)}$. Moreover, in the heavy nuclei of all atomic and molecular systems for which EDMs have been measured so far, the isoscalar and isovector contributions occur in approximately the same ratio, $(Z - N)/(Z + N) \approx -0.2$, so the effective parameter C_S is approximately system-independent. As noted above, we do not rely on these assumptions.

Next, we relate the pseudoscalar and tensor semileptonic interactions in a similar fashion. We start with the linear combinations for nucleons, $C_{P,T}^{(n,p)} = C_{P,T}^{(0)} \mp C_{P,T}^{(1)}$, where the upper sign refers to n according to our isospin convention. From those, the coefficients for a given nucleus can be constructed according to the sum over spins of the constituent nucleons, where $\langle \sigma_{p,n} \rangle$ represents the expectation value for neutrons or protons, evaluated via Pauli operators for the measured nuclear state [47, 48]:

$$C_{P,T} = \frac{C_{P,T}^{(n)} \langle \sigma_n \rangle + C_{P,T}^{(p)} \langle \sigma_p \rangle}{\langle \sigma_n \rangle + \langle \sigma_p \rangle}. \quad (16)$$

For C_T we can see from Eq.(13) that the isoscalar and isovector couplings differ only through the corresponding nucleon form factors. These are calculated with small theoretical uncertainties in lattice QCD [49], allowing us to write

$$C_T = \left(1 - \frac{g_T^{(1)}}{g_T^{(0)}} \frac{\langle \sigma_n \rangle - \langle \sigma_p \rangle}{\langle \sigma_n \rangle + \langle \sigma_p \rangle} \right) C_T^{(0)} \quad \text{with} \quad \frac{g_T^{(1)}}{g_T^{(0)}} \approx 1.7. \quad (17)$$

Similarly, for C_P it can be shown that

$$C_P = C_P^{(0)} - \frac{g_P^{(1)}}{g_S^{(0)}} \frac{\langle \sigma_n \rangle - \langle \sigma_p \rangle}{\langle \sigma_n \rangle + \langle \sigma_p \rangle} C_S^{(0)} \quad \text{with} \quad \frac{g_P^{(1)}}{g_S^{(0)}} \approx 20.2. \quad (18)$$

For the derivation of $g_P^{(1)}$ in this ratio we follow Ref. [14]. We consider only the first generation as relevant light quarks, such that $g_P^{(1)}$ is dominated by the π -pole contribution

$$g_P^{(1)} = \frac{g_A \bar{m}_N}{\bar{m}} \frac{m_\pi^2}{m_\pi^2 - q^2} + \text{heavy quarks} \quad \bar{m} = \frac{m_u + m_d}{2}. \quad (19)$$

Here $\bar{m}_N \approx 940$ MeV is the average nucleon mass, \bar{m} the average light quark mass, and g_A is the (isovector) axial vector coupling [50]. The coupling $g_P^{(0)}$, appearing in Eq.(15), involves the isoscalar axial coupling $g_A^{(0)}$, obtained from the sum rather than the difference of the light quark axial charges [51]. We extend this by including a light s -quark, where the π -pole dominance is replaced by an octet η -pole with an appropriately modified average light quark mass m^* ,

$$g_P^{(0)} = \frac{g_A^{(0)} \bar{m}_N}{m^*} \frac{m_\eta^2}{m_\eta^2 - q^2} + \text{heavy quarks} \quad m^* = \frac{\bar{m} + 2m_s}{3}. \quad (20)$$

Note that heavy quark contributions enter differently in $g_P^{(0)}$ and $g_P^{(1)}$, and can be derived using the $U(1)_A$ axial anomaly together with the divergence of the anomaly-free axial current $J_{\mu 5}^q = \bar{q} \gamma_\mu \gamma_5 q$ for all quarks q [51–55]. These represent a relatively minor contribution to $g_P^{(1)}$, but due to suppression of the η -pole relative to the π -pole by the factor m^*/\bar{m} , contribute to $g_P^{(0)}$ at approximately the same level as the light quarks.

Our final, simplifying assumption is not strictly needed, but is effective in reducing the number of model parameters by one and removing a poorly constrained direction in model space,

$$d_p \approx -d_n . \quad (21)$$

Alternatively, we could set $d_{n,p}^{sr}$, as described further in App. A. The nuclei of the measured closed-shell systems, which apart from the neutron itself provide the strongest constraints on nucleon EDMs, are typically dominated either by a valence proton (in the case of TlF) or a valence neutron (all others). In analogy with the anomalous magnetic moment, the short-range nucleon EDMs are assumed to be dominated by the isovector contribution. This assumption can be relaxed for the purposes of a rigorous global analysis, provided improved theory uncertainties concerning the contributions of all nucleons to the overall EDM of each measured system. Of the present experimental limits, TlF has the leading sensitivity to d_p . (Note that Cs also has a valence proton, whose contribution can be somewhat enhanced through a magnetic quadrupole moment [56,57]).

With the simplifications described in this section, the set of independent low-energy parameters given in Eq.(11) reduces to

$$c_j \in \left\{ d_e, C_S^{(0)}, C_T^{(0)}, C_P^{(0)}, g_\pi^{(0)}, g_\pi^{(1)}, d_n \right\} , \quad (22)$$

which are the model parameters for our global EDM analysis.

3 EDM Measurements

In terms of the Lagrangian parameters in Eq.(22) we can predict the measured EDMs d_i as linear combinations with system-specific coefficients α_{i,c_j} ,

$$d_i = \sum_{c_j} \alpha_{i,c_j} c_j . \quad (23)$$

The measurements we analyze are listed in Tab. 1 and discussed below. Unless otherwise indicated, the isotopes and charge states that we discuss are those given in Tab. 1. The isotopes that are relevant for these molecular systems are ^{180}Hf , ^{232}Th , ^{174}Yb , ^{205}Tl , ^{16}O , and ^{19}F . We neglect constraints from the comparatively weaker experimental bounds from ^{85}Rb [58,59], Xe^m [60], PbO [61], $\text{Eu}_{0.5}\text{Ba}_{0.5}\text{TiO}_3$ [62], and the Λ hyperon [63]. The experimental bounds for the μ and τ leptons constrain the corresponding Lagrangian parameters and factorize from the hadronic-scale Lagrangian. We do not include them in our first global analysis.

As discussed in the last section, the α -values for *all* $C_{S,P,T}^{(0,1)}$ are fixed by the corresponding values for the basis of Eq.(22). For this we follow Eqs. (15)-(18) and find for example

$$\begin{aligned} \alpha_{C_S^{(0)}} &= \alpha_{C_S} - \alpha_{C_P} \frac{g_P^{(1)} \langle \sigma_n \rangle - \langle \sigma_p \rangle}{g_S^{(0)} \langle \sigma_n \rangle + \langle \sigma_p \rangle} \\ \alpha_{C_P^{(0)}} &= \alpha_{C_P} + \alpha_{C_S} \frac{g_S^{(1)} Z - N}{g_P^{(0)} Z + N} \\ \alpha_{C_T^{(0)}} &= \left(1 - \frac{g_T^{(1)} \langle \sigma_n \rangle - \langle \sigma_p \rangle}{g_T^{(0)} \langle \sigma_n \rangle + \langle \sigma_p \rangle} \right) \alpha_{C_T} , \end{aligned} \quad (24)$$

System i	Measured d_i [e cm]	Upper limit on $ d_i $ [e cm]	Reference
n	$(0.0 \pm 1.1_{\text{stat}} \pm 0.2_{\text{syst}}) \cdot 10^{-26}$	$2.2 \cdot 10^{-26}$	[69]
^{205}Tl	$(-4.0 \pm 4.3) \cdot 10^{-25}$	$1.1 \cdot 10^{-24}$	[70]
^{133}Cs	$(-1.8 \pm 6.7_{\text{stat}} \pm 1.8_{\text{syst}}) \cdot 10^{-24}$	$1.4 \cdot 10^{-23}$	[71]
HfF^+	$(-1.3 \pm 2.0_{\text{stat}} \pm 0.6_{\text{syst}}) \cdot 10^{-30}$	$4.8 \cdot 10^{-30}$	[72]
ThO	$(4.3 \pm 3.1_{\text{stat}} \pm 2.6_{\text{syst}}) \cdot 10^{-30}$	$1.1 \cdot 10^{-29}$	[73]
YbF	$(-2.4 \pm 5.7_{\text{stat}} \pm 1.5_{\text{syst}}) \cdot 10^{-28}$	$1.2 \cdot 10^{-27}$	[74]
^{199}Hg	$(2.20 \pm 2.75_{\text{stat}} \pm 1.48_{\text{syst}}) \cdot 10^{-30}$	$7.4 \cdot 10^{-30}$	[75, 76]
^{129}Xe	$(-1.76 \pm 1.82) \cdot 10^{-28}$	$4.8 \cdot 10^{-28}$	[77, 78]
^{171}Yb	$(-6.8 \pm 5.1_{\text{stat}} \pm 1.2_{\text{syst}}) \cdot 10^{-27}$	$1.5 \cdot 10^{-26}$	[79]
^{225}Ra	$(4 \pm 6_{\text{stat}} \pm 0.2_{\text{syst}}) \cdot 10^{-24}$	$1.4 \cdot 10^{-23}$	[80]
TlF	$(-1.7 \pm 2.9) \cdot 10^{-23}$	$6.5 \cdot 10^{-23}$	[81]
	Measured ω_i [mrad/s]	Rescaling factor x_i for d_i	Reference
HfF^+	$(-0.0459 \pm 0.0716_{\text{stat}} \pm 0.0217_{\text{syst}})^{\dagger}$	0.999	[72]
ThO	$(-0.510 \pm 0.373_{\text{stat}} \pm 0.310_{\text{syst}})$	0.982	[73]
YbF	$(5.30 \pm 12.60_{\text{stat}} \pm 3.30_{\text{syst}})$	1.12	[74]

Table 1: Measured EDM values and 95% CL for upper limits on their absolute values. For ^{129}Xe we combine two independent results with similar precision, using inverse-variance weighting. For the open-shell molecules, we also provide the measured angular frequencies and the rescaling factor which allows us to use $x_i d_i$ for each experimentally reported d_i . For the definition of x_i , see text. † The frequency for HfF^+ is scaled by a factor of 2 relative to Ref. [72], to consistently use Eq.(30) for all systems.

with the $\alpha_{\text{CS},RT}$ given in Tab. 2. In this table we also show

$$\langle \sigma_z \rangle^{(0)} = \langle \sigma_n \rangle + \langle \sigma_p \rangle, \quad (25)$$

which is proportional to the isoscalar sum of neutron and proton spin projections in a shell model of the nucleus, a factor of two being given by the usual relation of the spin and Pauli operators. The shell model is not expected to be reliable for the deformed nuclei ^{171}Yb and ^{225}Ra . The values given in Tab. 2 are chosen to optimize agreement of the calculated and measured nuclear magnetic moments within this framework. Literature values are available for these nuclear species [48]. The spin fractions contributing to semileptonic coefficients in TlF only take into account the ^{205}Tl nucleus, though see Ref. [64] for some consideration of contributions from the ^{19}F nucleus. For $\alpha_{^{129}\text{Xe},\text{CS}}$ we use a scaling relation to derive a value from $\alpha_{^{129}\text{Xe},\text{CT}}$ of the cited reference.

With the exception of $\alpha_{^{129}\text{Xe},\text{CS}}$, we use only explicitly calculated values and employ the established phenomenological scaling relations only as consistency checks. For this one case, however, although a precise explicit calculation is available it deviates from both the scaling relations [65] and other explicit calculations [35] for presently unknown reasons. We therefore employ a scaled value of the explicitly calculated $\alpha_{^{129}\text{Xe},\text{CT}}$ [66], using the semianalytical relations of [56, 65, 67, 68].

System i	$\langle\sigma_n\rangle$	$\langle\sigma_p\rangle$	$\langle\sigma_z\rangle^{(0)}$	$\alpha_{i,C_S} [e \text{ cm}]$	$\alpha_{i,C_P} [e \text{ cm}]$	$\alpha_{i,C_T} [e \text{ cm}]$
Tl	0.274	0.726	1	$-6.77 \cdot 10^{-18}$ [82]	$1.5 \cdot 10^{-23}$ [83]	$5 \cdot 10^{-21}$ [83]
Cs	-0.206	-0.572	-0.778	$7.8 \cdot 10^{-19}$ [14]	$2.2 \cdot 10^{-23}$ [83]	$9.2 \cdot 10^{-21}$ [83]
^{199}Hg	-0.302	-0.032	-0.334	$-2.8 \cdot 10^{-22}$ [84]	$6 \cdot 10^{-23}$ [66]	$1.7 \cdot 10^{-20}$ [66]
^{129}Xe	0.73	0.27	1	$-6.28 \cdot 10^{-23}$ [66]	$1.6 \cdot 10^{-23}$ [66]	$5.7 \cdot 10^{-21}$ [66]
^{171}Yb	-0.3	-0.034	-0.334	$-7.34 \cdot 10^{-22}$ [35]	$3.60 \cdot 10^{-23}$ [35]	$1.04 \cdot 10^{-20}$ [35]
^{225}Ra	0.72	0.28	1	$5.63 \cdot 10^{-21}$ [35]	$-6.4 \cdot 10^{-22}$ [66]	$-1.8 \cdot 10^{-19}$ [66]
TlF	0.274	0.726	1	$1.09 \cdot 10^{-16}$ [35]	$3.8 \cdot 10^{-18}$ [35]	$1.06 \cdot 10^{-15}$ [85]

Table 2: Effective parameters used as input to our global analysis, as summarized in Tab. 3.

3.1 Nucleons

We start with the simplest hadronic systems for which we can measure EDMs, the nucleons. Their EDMs can be written directly as a Lagrangian term

$$-\frac{i}{2} F^{\mu\nu} d_N (\bar{N} \sigma_{\mu\nu} \gamma_5 N), \quad (26)$$

but can also be described by heavy baryon chiral perturbation theory, based on the hadronic-scale Lagrangian. In that case we can consider the nucleon EDMs as observables that receive contributions from: short-range contributions d_N^{sr} , NNLO pion-loop contributions, and potential direct contributions to Eq.(26) within and beyond the SM [86],

$$\begin{aligned} d_n &= d_n^{\text{sr}} - \frac{e g_A}{8\pi^2 F_\pi} \left[g_\pi^{(0)} \left(\ln \frac{m_\pi^2}{m_N^2} - \frac{\pi m_\pi}{2m_N} \right) - \frac{g_\pi^{(1)}}{4} (\kappa_0 - \kappa_1) \frac{m_\pi^2}{m_N^2} \ln \frac{m_\pi^2}{m_N^2} \right] \\ d_p &= d_p^{\text{sr}} + \frac{e g_A}{8\pi^2 F_\pi} \left[g_\pi^{(0)} \left(\ln \frac{m_\pi^2}{m_N^2} - \frac{2\pi m_\pi}{m_N} \right) - \frac{g_\pi^{(1)}}{4} \left(\frac{2\pi m_\pi}{m_N} + \left(\frac{5}{2} + \kappa_0 + \kappa_1 \right) \frac{m_\pi^2}{m_N^2} \ln \frac{m_\pi^2}{m_N^2} \right) \right], \end{aligned} \quad (27)$$

where $F_\pi = 92 \text{ MeV}$ is the pion decay constant [87], $m_\pi = 139 \text{ MeV}$, $m_N = 940 \text{ MeV}$, $g_A \approx 1.27$ is the nucleon isovector axial charge, and the isoscalar and isovector nucleon anomalous magnetic moments are $\kappa_0 = -0.12$ and $\kappa_1 = 3.7$. We set the renormalization scale to the nucleon mass, and the splitting between proton and neutron masses leads to a higher-order effect that is presently negligible in relation to other uncertainties. In terms of weak-scale parameters, finite values of $g_\pi^{(0,1)}$ can be related to a CKM phase or $\bar{\theta}$, but also to 4-fermion quark operators. The input from the presently most sensitive neutron EDM measurement to our global analysis is given in Tab. 1, alongside the other measurements we use.

From Eq.(27) is it clear that we have a choice of defining either $d_{n,p}^{\text{sr}}$ or $d_{n,p}$ as our model parameters. Constraints on these Lagrangian parameters, including a renormalization condition, are the output of our global analysis; but their real purpose is to compute yet other observables, and compare them to measurements within a consistent theory.

The two choices are not equivalent any longer, when we remove d_p or d_p^{sr} . Choosing $d_{n,p}$ as model parameters implies that we use measured values as Lagrangian parameters. The corresponding renormalization condition is referred to as on-shell renormalization in collider physics. In that case, we can extract d_n and d_p from data and use Eq.(27) to translate them into $d_{n,p}^{\text{sr}}$. We use this scheme in the main body of the paper. The alternative of using $d_{n,p}^{\text{sr}}$ as model parameters may be a better motivation to use the approximate relation $d_p^{\text{sr}} = -d_n^{\text{sr}}$ rather than Eq.(21). We present a complete set of results using this approach in the Appendix.

Neither of the two renormalization conditions allows for a simple running of the Lagrangian parameters to higher scales. For this third option we must renormalize d_N in the $\overline{\text{MS}}$ scheme and compute the difference, in analogy to Eq.(27), in perturbation theory.

3.2 Open-shell (paramagnetic) systems

Atoms and molecules with open electronic shells, sometimes also referred to as paramagnetic² systems, are primarily sensitive to the electron EDM and the scalar electron-nucleon couplings $C_S^{(0,1)}$ of Eq.(10). It is common to distinguish the case of open-shell atoms with the atomic EDMs

$$d_i = \alpha_{i,d_e} d_e + \alpha_{i,C_S} C_S + \dots \quad \text{for} \quad i \in \{\text{Ti, Cs}\} \quad (28)$$

from that of open-shell molecules, although in both cases the terms involving the Lagrangian parameters d_e and C_S dominate. The experimentally relevant quantity is a phase difference accumulated over some measurement time, interpreted as a frequency. Measurements with open-shell molecules are often reported as a parity- and time-reversal-violating frequency shift ω_i ,

$$\omega_i = \eta_{i,d_e}^{(m)} d_e + k_{i,C_S}^{(m)} C_S + \dots \quad \text{for} \quad i \in \{\text{HfF}^+, \text{ThO}, \text{YbF}\}. \quad (29)$$

The superscript (m) indicates the molecular systems. We also give these measured angular frequencies in Tab. 1. This emphasizes that ω_i does not scale in a simple way with the experimentally applied electric field; it rather depends on the molecular structure via a so-called effective electric field E_{eff} that saturates when the molecule is polarized. Note that α_{i,d_e} is dimensionless, while $\eta_{i,d_e}^{(m)}$ is not; similarly α_{i,C_S} has the units of an EDM, while $k_{i,C_S}^{(m)}$ has units of angular frequency.

The remaining contributions to open-shell molecular EDMs have weak dependences on other low-energy constants, and we note that in particular the EDMs of the μ and τ leptons have been indirectly constrained via the experimental limits from ThO and Hg [101]. However, we are not aware of any established values for the coefficients of semileptonic or hadronic parameters. (Note that due to the vanishing nuclear spin of ^{232}Th , ^{180}Hf , and ^{174}Yb there is no leading contribution to the system EDM from C_P or C_T for the heavy nucleus in any of the measured open-shell molecules.) We thus take $\alpha_{i,c_j}^{(m)} = 0$ in Eq.(29), while for the open-shell atoms we obtain values for semileptonic coefficients either from the literature or by scaling arguments, as reported in Tabs. 2 and 3.

Now starting with the truncated version of Eq.(29), we adopt the convention that

$$\begin{aligned} \omega_i &= \eta_{i,d_e}^{(m)} d_e + k_{i,C_S}^{(m)} C_S \\ &= -\frac{E_{\text{eff},i}}{\hbar} d_e + \frac{W_i}{\hbar} C_S, \end{aligned} \quad (30)$$

where all signs, g -factors, spin magnitudes, etc. are absorbed into the coefficients on the right-hand side. It is also common to refer to \mathcal{E}_{eff} as the effective electric field, where

$$E_{\text{eff}} = \mathcal{E}_{\text{eff}} \text{sgn}(\vec{J} \cdot \hat{n}) \langle \hat{n} \cdot \hat{z} \rangle, \quad (31)$$

²We prefer the nomenclature of open-shell and closed-shell systems, rather than paramagnetic or diamagnetic, since this more clearly indicates the properties that are relevant for determining the leading contributions to the total system EDM.

System i	α_{i,d_e}	$\alpha_{i,C_S^{(0)}} [e \text{ cm}]$	$\alpha_{i,C_P^{(0)}} [e \text{ cm}]$	$\alpha_{i,C_T^{(0)}} [e \text{ cm}]$	$\alpha_{i,g_\pi^{(0)}} [e \text{ cm}]$	$\alpha_{i,g_\pi^{(1)}} [e \text{ cm}]$	α_{i,d_n}	α_{i,d_p}
n	—	—	—	—	0	0	1	(−1)
^{205}Tl	-558^{+28}_{-18} [88]	$-6.77^{+0.34}_{-0.8} \cdot 10^{-18}$	$1.4^{+2.5}_{-0.8} \cdot 10^{-19}$	$8.8^{+4.0}_{-1.2} \cdot 10^{-21}$	$-6.41^{+3.57}_{-4.51} \cdot 10^{-18}$	$2.27^{+6.13}_{-1.19} \cdot 10^{-19}$	$-5.75^{+3.44}_{-4.44} \cdot 10^{-6}$	$1.61^{+3.35}_{-7.56} \cdot 10^{-5}$
^{133}Cs	123^{+4}_{-4} [16, 84]	$7.80^{+0.2}_{-0.8} \cdot 10^{-19}$	$-1.4^{+0.8}_{-2.2} \cdot 10^{-20}$	$1.7^{+0.4}_{-0.4} \cdot 10^{-20}$	$8.09^{+15.1}_{-2.63} \cdot 10^{-19}$	$2.70^{+3.27}_{-1.79} \cdot 10^{-18}$	$1.0^{+1}_{-1} \cdot 10^{-5}$	$6.7^{+2}_{-2} \cdot 10^{-4}$
^{199}Hg	$11.6^{+10}_{-8} \cdot 10^{-3}$ [35, 89]	$-1.26^{+0.7}_{-1.5} \cdot 10^{-21}$	$6.6^{+2.4}_{-0.5} \cdot 10^{-23}$	$-6.4^{+3}_{-0.78} \cdot 10^{-21}$	$-3.05^{+1.75}_{-1.45} \cdot 10^{-18}$	$-6.10^{+16.6}_{-25.3} \cdot 10^{-18}$	$-1.36^{+0.38}_{-0.57} \cdot 10^{-4}$	$-1.36^{+0.38}_{-0.57} \cdot 10^{-5}$
^{129}Xe	$-8^{+16}_{-8} \cdot 10^{-4}$ [35, 89]	$-2.1^{+1.5}_{-2.5} \cdot 10^{-22}$	$1.7^{+0.5}_{-0.4} \cdot 10^{-23}$	$1.24^{+0.78}_{-0.61} \cdot 10^{-21}$	$-3.91^{+1.45}_{-23.4} \cdot 10^{-19}$	$2.93^{+1.64}_{-7.74} \cdot 10^{-19}$	$2.29^{+0.57}_{-0.58} \cdot 10^{-5}$	$4.89^{+1.24}_{-1.25} \cdot 10^{-6}$
^{171}Yb	$1.44^{+165}_{-4.5} \cdot 10^{-3}$ [35]	$-1.31^{+0.35}_{-1.05} \cdot 10^{-21}$	$4.93^{+3.54}_{-1.55} \cdot 10^{-23}$	$-3.68^{+1.86}_{-2.43} \cdot 10^{-21}$	$-2.84^{+0.43}_{-6.95} \cdot 10^{-18}$	$-5.67^{+7.74}_{-10.3} \cdot 10^{-18}$	$-1.13^{+0.32}_{-0.28} \cdot 10^{-4}$	$-1.13^{+0.32}_{-0.28} \cdot 10^{-5}$
^{225}Ra	$-5.4^{+134}_{-2.0} \cdot 10^{-2}$ [35]	$1.13^{+2.94}_{-0.53} \cdot 10^{-20}$	$-7.63^{+2.05}_{-3.88} \cdot 10^{-22}$	$-4.5^{+2.0}_{-2.5} \cdot 10^{-20}$	$1.72^{+5.73}_{-9.67} \cdot 10^{-15}$	$-6.89^{+2.66}_{-2.29} \cdot 10^{-15}$	$-5.38^{+1.20}_{-1.58} \cdot 10^{-4}$	$-1.19^{+0.27}_{-0.35} \cdot 10^{-4}$
TlF	$1.36^{+2.0}_{-0.32} \cdot 10^3$ [35]	$1.44^{+0.5}_{-0.5} \cdot 10^{-16}$	$1.51^{+3.82}_{-3.6} \cdot 10^{-18}$	$1.87^{+0.17}_{-0.17} \cdot 10^{-15}$	$-7.00^{+3.17}_{-2.17} \cdot 10^{-13}$	$2.48^{+0.34}_{-0.34} \cdot 10^{-14}$	$-6.28^{+1.58}_{-2.28} \cdot 10^{-1}$	$1.76^{+2.41}_{-0.76}$
HfF ⁺	1	$9.17^{+0.06}_{-0.06} \cdot 10^{-21}$	—	—	—	—	—	—
ThO	1	$1.51^{+0}_{-0.2} \cdot 10^{-20}$	—	—	—	—	—	—
YbF	1	$8.99^{+0.70}_{-0.70} \cdot 10^{-21}$	—	—	—	—	—	—
	$\eta_{i,d_e}^{(m)} \left[\frac{\text{mrad}}{\text{s e cm}} \right]$	$k_{i,C_S}^{(m)} \left[\frac{\text{mrad}}{\text{s}} \right]$	α_{i,C_P}	α_{i,C_T}	$\alpha_{i,g_\pi^{(0)}}$	$\alpha_{i,g_\pi^{(1)}}$	α_{i,d_n}	α_{i,d_p}
HfF ⁺	$3.49^{+0.14}_{-0.14} \cdot 10^{28}$ [84, 90–93]	$3.2^{+0.1}_{-0.2} \cdot 10^8$ [84, 90, 91]	—	—	—	—	—	—
ThO	$-1.21^{+0.05}_{-0.39} \cdot 10^{29}$ [84, 94–96] [†]	$-1.82^{+0.42}_{-0.27} \cdot 10^9$ [84, 94, 96–98] [†]	—	—	—	—	—	—
YbF	$-1.96^{+0.15}_{-0.15} \cdot 10^{28}$ [84, 97–100]	$-1.76^{+0.2}_{-0.2} \cdot 10^8$ [84, 97–99]	—	—	—	—	—	—

Table 3: Central values and theory uncertainties for the α -parameters defined in Eq. (23), using $d_{n,p}$ as model parameters. The parentheses around α_{n,d_p} indicate our assumption Eq. (21), i.e., this value should not be construed as entering Eq. (23). (For the implementation using $d_{n,p}^{\text{sr}}$, see Appendix A and in particular Tab. 6.) Here entries given only as “—” indicate that we neglect the dependence in our global analysis, e.g., because that coefficient arises only for nuclei with spin. [†]There appears to be an overall sign error in the coefficients reported for ThO in Table 4 of Ref. [84]. The values for Tl and Cs of $\alpha_{i,C_T^{(0)}}$ are estimated by simple analytical calculations [83], and the uncertainties quoted here are estimated as approximately twice those arising from the relevant hadronic matrix elements.

and \vec{J} is the total electronic angular momentum, \hat{n} is the direction of the internuclear axis, and \hat{z} is the direction of the externally applied electric field. Here $\Omega = \vec{J} \cdot \hat{n}$ is a quantum number used in molecular term symbols, and $\langle \hat{n} \cdot \hat{z} \rangle$ indicates the degree to which the molecule is electrically polarized by the applied electric field. Some of the conventions used for the orientation of the internuclear axis, the internal electric field, etc. are summarized in Appendix A.3 of Ref. [102].

The truncated expression for the frequency shift thus provides us with physical expressions for the two constants,

$$\eta_{i,d_e}^{(m)} = -\frac{E_{\text{eff},i}}{\hbar} \quad \text{and} \quad k_{i,C_S}^{(m)} = \frac{W_i}{\hbar}. \quad (32)$$

The point is that this frequency measurement cannot be directly translated into a permanent molecular dipole moment, since the molecules are substantially or entirely electrically polarized during the measurement. The linear energy shift due to the lab-frame electric field saturates as $\langle \hat{n} \cdot \hat{z} \rangle \rightarrow 1$, and the limiting dependence on the external fields is that of an induced dipole moment. To express the frequency difference ω_i in terms of a physically meaningful permanent electric dipole moment, we define the molecule's d_i in relation to the effective electric field,

$$-E_{\text{eff},i} d_i \equiv -E_{\text{eff},i} d_e + W_i C_S. \quad (33)$$

We can use this form to define, in analogy to Eq.(28),

$$d_i = d_e + \alpha_{i,C_S} C_S \quad \Leftrightarrow \quad \alpha_{i,d_e} = 1 \quad \text{and} \quad \alpha_{i,C_S} = -\frac{W_i}{E_{\text{eff},i}} = \frac{k_{i,C_S}^{(m)}}{\eta_{i,d_e}^{(m)}}. \quad (34)$$

For our analysis we re-cast the limits from open-shell molecules in units of ecm , such that the coefficients for all systems can be expressed in the same units, with the side effect that $\alpha_{i,d_e} = 1$ for all open-shell molecules. This approach also serves two additional purposes: (i) Many different conventions are in use for these coefficients, sometimes using the same symbols for different quantities. Since measured quantities are related in publications to the electron EDM, our choice makes comparisons across different works relatively straightforward. Of course, all quantities must be ultimately connected to an experimentally measured phase. (ii) As first pointed out in Refs. [97, 98], while there is considerable variation in the literature values for $\eta_{i,d_e}^{(m)}$ and $k_{i,C_S}^{(m)}$ in a given system, there is much less variation in their ratio. Dividing Eq.(29) by $\eta_{i,d_e}^{(m)}$ should pass this uncertainty on to all semileptonic and hadronic coefficients, which are of much less relevance in open-shell systems.

Note that $\eta_{i,d_e}^{(m)}$ is used both to obtain single-source limits on d_e from the experimentally measured ω_i , and to convert the experimentally measured frequencies into EDM units for Tab. 1. The experimental EDM limits for open-shell molecules in Tab. 1 are rescaled by the indicated factor x_i , which differs from unity when updated values for $\eta_{i,d_e}^{(m)}$ differ from the cited publication. This is typically the case when improved molecular structure calculations have become available since the experimental limit was published.

Recommended values for many of the α_{i,c_j} are given in Tables III-V of Ref. [16] and in Table 4 of Ref. [84], including in many cases the ranges corresponding to theory uncertainties (or at least the ranges of reported values, which is often what we are forced to use in lieu of true theory uncertainties). We give our choices for α_{i,c_j} in Tab. 3.

3.3 Closed-shell (diamagnetic) systems

In contrast to the open-shell systems, where sub-leading contributions are largely neglected due to lack of theory inputs, the small contributions of d_e and $C_S^{(0)}$ are taken into account for all closed-shell systems. These are typically smaller contributions to the observable EDM in cases where all electron spins are paired, with the main contributions coming rather from nucleon EDMs, nuclear forces mediated by pion exchange with strengths $g_\pi^{(0,1,2)}$, and the nuclear-spin-dependent semileptonic interactions $C_T^{(0)}$ (and possibly $C_P^{(0)}$). The experimental precision, especially of Hg, is nevertheless high enough to contribute meaningful constraining power for d_e and $C_S^{(0)}$.

Unfortunately it appears that arguments [84] to the effect that closed-shell systems add significant complementary constraining power in the $d_e - C_S$ subspace due to a different sign of the ratio $\alpha_{i,d_e}/\alpha_{i,C_S}$ in comparison to open-shell systems, do not in fact hold. While recent calculations [35] may indicate that α_{i,d_e} and α_{i,C_S} in some highly-correlated closed-shell systems could indeed have different sign, the theory uncertainties for these cases are large enough to cross zero. Numerical calculations for specific systems so far only support ratios of the same sign [103]. Two subtleties are important to consider in this context: (1) the value for α_{i,d_e} includes contributions from multiple different interactions [35, 66, 89, 104] whose contributions must be summed, and (2) our implementation of $\alpha_{C_S^{(0)}}$ could generate sign changes via the difference of terms in equation 24.

At present, as can be seen from Tabs 2 and 3, the only measured system where α_{i,d_e} and α_{i,C_S} may have opposite sign are Hg, Yb, and Ra. On the other hand, the allowed ranges for α_{i,d_e} cross zero, and thus admit also a positive ratio as in all other systems discussed here. These may thus represent special cases among closed-shell systems, in that reducing the error of experimental and theory inputs could have significant impact on the $d_e - C_S^{(0)}$ subspace that is complementary to the dominating open-shell constraints. The supporting arguments for any such claims should, however, be examined in detail.

The contributions of nuclear forces and nucleon EDMs are frequently interpreted via the Schiff moment of a given nucleus [16, 56, 105], which is more easily related to nuclear structure parameters [57, 83]. In terms of our model coefficients, the Schiff moment S_i of system i and a system-specific coefficient $k_{i,S}$ can be expressed related to the corresponding EDM via

$$\begin{aligned} k_{i,S} S_i &= \sum_{c_j \in \{d_{n,p}, g_\pi^{(0,1,2)}\}} \alpha_{i,c_j} c_j \\ &\approx k_{i,S} \left[s_{i,n} d_n + s_{i,p} d_p + \frac{m_N g_A}{F_\pi} (a_{i,0} g_\pi^{(0)} + a_{i,1} g_\pi^{(1)} + a_{i,2} g_\pi^{(2)}) \right] \\ &= k_{i,S} \left[s_{i,n} d_n^{\text{sr}} + s_{i,p} d_p^{\text{sr}} + \frac{m_N g_A}{F_\pi} (\tilde{a}_{i,0} g_\pi^{(0)} + \tilde{a}_{i,1} g_\pi^{(1)} + \tilde{a}_{i,2} g_\pi^{(2)}) \right]. \end{aligned} \quad (35)$$

The coefficients $s_{i,N}$ ($N = n, p$) indicate the contributions from EDMs of unpaired nucleons and the coefficients $a_{i,m}$ ($m = 0, 1, 2$) parameterize the strength of CP-violating pion exchange, organized by isospin, for the nucleus of system i . We drop the $g_\pi^{(2)}$ term as discussed above and note that the coefficients in front of $g_\pi^{(0)}$ and $g_\pi^{(1)}$ change when we replace $d_{n,p}$ with $d_{n,p}^{\text{sr}}$ using Eq.(27) (i.e., $a_{i,j} \neq \tilde{a}_{i,j}$). While we continue to neglect C_1 and C_2 from Eq.(9), these also contribute to the Schiff moment (the sensitivity coefficients for most measured species have not, however, been calculated). The coefficients $k_{i,S}$ are calculated for many systems of interest, and give the degree of electronic screening that suppresses an observable system EDM relative to its underlying nuclear Schiff moment. The Schiff moment itself can, in principle, be large in heavy and especially deformed nuclei such as ^{225}Ra . This can be viewed as a

nuclear-structure induced enhancement of the observable EDM, which affects not only the pion-exchange forces but also the nucleon EDMs and other contributions to S_i .

For nuclei with spin $I > 1/2$, a CP-violating nuclear magnetic quadrupole moment (MQM) can in principle exist in analogy to a Schiff-moment-induced EDM and be analyzed within a common global analysis (the MQM actually induces a higher-order correction to S_i). The MQM is *not* screened, and itself represents an experimentally useful signature of CP violation that we do not consider here in detail (but see [56, 83, 106]). At present, of the experimental systems already measured, this effect is relevant essentially only for Cs.

Among the potentially leading contributions from our six hadronic-scale model parameters $C_{pT}^{(0)}$, $d_{n,p}$, and $g_\pi^{(0,1)}$, very different weights can arise according to the electronic and nuclear structure of the various closed-shell systems. Inspecting Tab. 3 reveals that to a limited extent, this is indeed already the case for the systems already measured. However, this complementarity is not yet fully exploited and should be the target of further study.

Despite the pion pole enhancement, $C_p^{(0)}$ appears suppressed relative to $C_T^{(0)}$ in all measured systems. The coefficients of $g_\pi^{(0,1)}$ are typically of comparable size for a given system, although possibly different in sign. Unfortunately the coefficients of $d_{n,p}$ are not well known for most nuclei, although in principle these can be calculated. For the pion-exchange forces, even in nuclei that have been the object of many studies, the theory uncertainties are large. This is especially true for soft nuclei such as our Hg and Xe, in which non-static deformations can present special challenges.

As part of a global analysis, a large number of experimental measurements from complementary closed-shell systems can disentangle contributions from model parameters that are relevant at some level for all of them. In this sense the role of d_e and $C_S^{(0)}$ takes on a new importance, not only to further constrain these parameters themselves, but also as an additional contribution to the EDM that brings along uncertainties which dilute the constraining power for other model parameters. Closed-shell molecular systems such as TlF, or molecular systems containing Schiff-enhanced nuclides, introduce complementary constraining power to our global analysis.

We finally note that closed-shell systems unite theory inputs from several quite different communities. Different conventions for assigning a negative isospin projection in the nucleon doublet have to be carefully noted when combining calculated coefficients from different sources, especially when we include semileptonic interactions together with nuclear forces. Reference [107] makes an effort to disambiguate a part of this issue for $\alpha_{g_\pi^{(0,1,2)}, 129\text{Xe}}$.

It is only possible to establish meaningful constraints in a context where the notation and conventions are clear, and where the uncertainties associated with theory inputs have been clearly assessed. Table 5 in the appendix gives the literature values and references, adapted as needed for consistency within our framework here, that we have used to produce Tabs 3 and 6 for actually performing a global analysis.

3.4 Single parameter ranges

In this section we provide single-source ranges for the individual model parameters of Eq. (22) plus the proton EDM,

$$c_j \in \left\{ d_e, C_S^{(0)}, C_T^{(0)}, C_p^{(0)}, g_\pi^{(0)}, g_\pi^{(1)}, d_n, d_p \right\}, \quad (36)$$

They are derived from each measured system by neglecting all other parameters that could contribute to that system's EDM. To extract these single-parameter ranges, we use isolated

terms from Eq.(23) for each EDM measurement listed in Tab. 1 and the model dependence from Tab. 3. For the likelihood we assume a Gaussian form, which means that all limits are quoted as symmetric one-sigma error bars around the central, best-fit value. While these single-parameter limits allow us to compare the reach of different measurements for CP violation as a whole, they do not give the allowed ranges of the individual model parameters. The reason is that contributions from different model parameters to the same measurement can cancel. Because an EFT builds on the assumption that many higher-dimensional operators are induced by a given physics model, the apparent constraining power of single-parameter limits is overly optimistic.

Using the single-parameter constraints in Tab. 4 we can compare the impact of different EDM measurements on a given model parameter, with the caveat that multi-dimensional correlations might change that picture. Starting with the electron EDM d_e , the open-shell molecules HfF^+ and ThO provide the strongest constraints, while the open-shell YbF molecule has a similar constraining power as the closed-shell Hg . The same two open-shell molecules are most constraining for the scalar electron-nucleon coupling $C_S^{(0)}$, again followed by Hg , YbF , and Tl .

The pseudoscalar and tensor electron-nucleon couplings $C_{p,T}^{(0)}$ can be probed by the open-shell atoms and the closed-shell systems. This is done at present by far most efficiently with Hg and then, with much reduced constraining power, by Tl , Xe , and TlF . It is difficult to estimate the impact of these measurements on the combination of $C_p^{(0)}$ and $C_T^{(0)}$, and we will see in the next section how this more complex dependence affects the full global analysis.

The four hadronic parameters, $g_\pi^{(0,1)}$ and $d_{n,p}$, are most strongly constrained by the neutron EDM measurement and again Hg , suggesting that there will be significant correlations between the leptonic and hadronic model parameters in the global analysis. The other closed-shell sys-

System i	$d_e [e \text{ cm}]$	$C_S^{(0)}$	$C_p^{(0)}$	$C_T^{(0)}$
Tl	$(7.2 \pm 7.7) \cdot 10^{-28}$	$(5.9 \pm 6.4) \cdot 10^{-8}$	$(-2.9 \pm 3.1) \cdot 10^{-6}$	$(-4.5 \pm 4.9) \cdot 10^{-5}$
Cs	$(-1.5 \pm 5.6) \cdot 10^{-26}$	$(-2.3 \pm 8.9) \cdot 10^{-6}$	$(1.3 \pm 5.0) \cdot 10^{-4}$	$(-1.1 \pm 4.1) \cdot 10^{-4}$
^{199}Hg	$(1.9 \pm 2.7) \cdot 10^{-28}$	$(-1.7 \pm 2.5) \cdot 10^{-9}$	$(3.3 \pm 4.7) \cdot 10^{-8}$	$(-3.4 \pm 4.9) \cdot 10^{-10}$
^{129}Xe	$(2.2 \pm 2.3) \cdot 10^{-25}$	$(8.4 \pm 8.7) \cdot 10^{-7}$	$(-1.0 \pm 1.1) \cdot 10^{-5}$	$(-1.4 \pm 1.5) \cdot 10^{-7}$
^{171}Yb	$(-4.7 \pm 3.6) \cdot 10^{-24}$	$(5.2 \pm 4.0) \cdot 10^{-6}$	$(-1.4 \pm 1.1) \cdot 10^{-4}$	$(1.8 \pm 1.4) \cdot 10^{-6}$
^{225}Ra	$(-0.7 \pm 1.1) \cdot 10^{-22}$	$(3.5 \pm 5.3) \cdot 10^{-4}$	$(-5.2 \pm 7.9) \cdot 10^{-3}$	$(-0.9 \pm 1.3) \cdot 10^{-4}$
TlF	$(-1.3 \pm 2.1) \cdot 10^{-26}$	$(-1.2 \pm 2.0) \cdot 10^{-7}$	$(-1.1 \pm 1.9) \cdot 10^{-5}$	$(-0.9 \pm 1.6) \cdot 10^{-8}$
HfF^+	$(-1.3 \pm 2.1) \cdot 10^{-30}$	$(-1.4 \pm 2.3) \cdot 10^{-10}$		
ThO	$(4.3 \pm 4.0) \cdot 10^{-30}$	$(2.8 \pm 2.7) \cdot 10^{-10}$		
YbF	$(-2.4 \pm 5.9) \cdot 10^{-28}$	$(-2.7 \pm 6.6) \cdot 10^{-8}$		
	$g_\pi^{(0)}$	$g_\pi^{(1)}$	$d_n [e \text{ cm}]$	$d_p [e \text{ cm}]$
Tl	$(6.2 \pm 6.7) \cdot 10^{-8}$	$(-1.8 \pm 1.9) \cdot 10^{-6}$	$(7.0 \pm 7.5) \cdot 10^{-20}$	$(-2.5 \pm 2.7) \cdot 10^{-20}$
Cs	$(-2.2 \pm 8.6) \cdot 10^{-6}$	$(-0.7 \pm 2.6) \cdot 10^{-6}$	$(-1.8 \pm 6.9) \cdot 10^{-19}$	$(-0.3 \pm 1.0) \cdot 10^{-20}$
^{199}Hg	$(-0.7 \pm 1.0) \cdot 10^{-12}$	$(-3.6 \pm 5.1) \cdot 10^{-13}$	$(-1.6 \pm 2.3) \cdot 10^{-26}$	$(-1.6 \pm 2.3) \cdot 10^{-25}$
^{129}Xe	$(4.5 \pm 4.7) \cdot 10^{-10}$	$(6.0 \pm 6.2) \cdot 10^{-10}$	$(-7.7 \pm 7.9) \cdot 10^{-24}$	$(-3.6 \pm 3.7) \cdot 10^{-23}$
^{171}Yb	$(2.4 \pm 1.8) \cdot 10^{-9}$	$(1.2 \pm 0.9) \cdot 10^{-9}$	$(6.0 \pm 4.6) \cdot 10^{-23}$	$(6.0 \pm 4.6) \cdot 10^{-22}$
^{225}Ra	$(2.3 \pm 3.5) \cdot 10^{-9}$	$(-5.8 \pm 8.7) \cdot 10^{-10}$	$(-0.7 \pm 1.1) \cdot 10^{-20}$	$(-3.4 \pm 5.0) \cdot 10^{-20}$
TlF	$(2.4 \pm 4.1) \cdot 10^{-11}$	$(-0.7 \pm 1.2) \cdot 10^{-9}$	$(2.7 \pm 4.6) \cdot 10^{-23}$	$(-1.0 \pm 1.6) \cdot 10^{-23}$

Table 4: Single-parameter ranges allowed by each of the EDM measurements given in Tab. 1 and coefficients from Tab. 3. The neutron EDM itself is best constrained by the direct experimental measurement using neutrons, see Tab. 1.

tems lead to much weaker limits, but are still needed to constrain the 3-dimensional hadronic model space. Note that we fix the relation between the short-range neutron and proton parameters in the Lagrangian, Eq.(21), but from Tab. 3 we know that different measurements probe different admixtures of these two parameters.

4 Global analysis

To jointly analyze the available EDM measurements in terms of the hadronic-scale Lagrangian and its parameters, Eq.(22), we use the established SFITTER analysis tool. It constructs a global likelihood with a comprehensive uncertainty treatment and analyses it in terms of high-dimensional correlations. Lower-dimensional and one-dimensional likelihoods for the individual model parameters can be derived by profiling or marginalization, depending on the preferred statistical framework. If we assume that experimental uncertainties are Gaussian, profiling and marginalization have to lead to identical results. For the theory uncertainties, discussed in Sec. 4.5, the difference between the two approaches makes a formal, but not significant difference.

4.1 SFitter framework

SFITTER [36–38] has been developed for global analyses of LHC measurements in the context of BSM physics [108] and Higgs and top properties [40, 109–111], including comprehensive studies of the connection between EFTs and UV-completions of the SM [112, 113]. It has a focus on its uncertainty treatment, including theory uncertainties [41], the connection between Bayesian and frequentist approaches [37, 39], and published experimental likelihoods [40].

This first SFITTER analysis of EDMs relates the 11 measurements from Tab. 1 to the seven model parameters in Eq.(22). In general, SFITTER includes statistical, systematic, and theory uncertainties. At the heart of SFITTER is the fully exclusive likelihood as a function of model and nuisance parameters. All measurements are described as uncorrelated, with the individual statistical uncertainties described by Poisson or Gaussian likelihood. Statistical uncertainties are, usually, uncorrelated as well and described by a Poisson distribution, turning into a Gaussian for high statistics. Experimental systematics are assumed to have a Gaussian shape, but can be described by any nuisance parameter. This Gaussian shape is justified for parameters which are measured elsewhere. We use it for all experimental uncertainties, assuming that the measurements are at least as much dominated by statistical uncertainty, with error distribution appropriate for count-rate limited frequency measurements.

For the EDM analysis the situation is then relatively simple. First, from Eq.(23) we know that all observables depend on the model parameters linearly. Second, we can combine the statistical and systematic experimental uncertainties into the symmetric Gaussian error bars given in Tab. 1. Finally, we do not have to consider nuisance parameters, if we assume that the likelihood has a Gaussian form for each independent measurement. This Gaussian assumption also implies that for uncorrelated uncertainties a profile likelihood and a Bayesian marginalization will give the same result.

In our implementation theory uncertainties have no well-defined likelihood shape, and no maximum: they can be thought of as a range of allowed values [41]. A flat theory uncertainty is not parametrization-invariant, as one would expect from a fixed range, but without a preferred central value, we consider it conservative. With this implementation in SFITTER following a flat distribution, the central value of the parameter can be shifted within this range at no cost

in the likelihood. Therefore, compared to analyses without considering theory uncertainties, the impact of the central value of certain parameters is negligible for larger ranges allowed by theory uncertainties. For the EDM global analysis, theory uncertainties significantly affect most α -values: the central values given in Tab. 3 mainly impact implementations that neglect theory uncertainties, while the corresponding ranges are by far more relevant when theory uncertainties are taken into account.

To construct the exclusive likelihood, SFITTER evaluates EDM predictions over the entire model parameter space. It uses a Markov chain to encode the likelihood in the distribution of points covering the model space. A helpful aspect, common to many BSM analyses, is that we can safely assume the global minimum of the likelihood to be at the SM parameter point. To remove nuisance parameters or to extract limits on a reduced number of model parameters, SFITTER can employ a profile likelihood or a Bayesian marginalization [37, 39]. These two methods give different results, with the exception of uncorrelated Gaussians. Profiling over flat theory uncertainties and Gaussian experimental uncertainties leads to the RFit [114] prescription, profiling over two parameters with flat likelihood leads to linearly added uncertainties even for uncorrelated parameters.

The typical sizes of the model parameters in Eq.(22) and the α -values in Tab. 3 can be extremely different. For numerical robustness, we internally re-scale each model parameter and each α -value such that all model parameters are evaluated with similar size (while each term in Eq. (23) remains invariant). Concretely, this means rescaling d_e by a factor 10^{29} , $C_S^{(0)}$ by 10^9 , $g_\pi^{(1)}$ and $g_\pi^{(0)}$ by 10^{10} , $C_T^{(0)}$ by 10^8 , $C_P^{(0)}$ by 10^6 , and $d_{n/p}$ by 10^{23} . These rescalings are also reflected in the way we present our results.

4.2 Well-constrained model sub-space

As a starting point of the global analysis and to understand the main features, we consider a subspace of relatively well-constrained parameters. Following our discussion in Sec. 3.4 we expect d_e and $C_S^{(0)}$ to be constrained well by the open-shell molecules HfF^+ and ThO . Similarly, the hadronic parameters $g_\pi^{(0)}$ and d_n are strongly constrained by the neutron and Hg EDMs. This means the model subspace

$$\{d_e, C_S, g_\pi^{(0)}, d_n\} \quad (37)$$

should be constrained well by the full set of measurements given in Tab. 1.

It is instructive to consider how the constraints on these four model parameters are correlated. In Fig. 1 we show these correlations extracted as 2-dimensional profile likelihoods from the fully exclusive, 4-dimensional likelihood. Three structural aspects are evident: (i) a strong anti-correlation between d_e and $C_S^{(0)}$; (ii) a very slight anti-correlation between $g_\pi^{(0)}$ and d_n ; and (iii) essentially no correlations linking the $\{d_e, C_S^{(0)}\}$ and $\{g_\pi^{(0)}, d_n\}$ parameter subsets.

The strong correlation between d_e and $C_S^{(0)}$ and its independence from the remaining parameter space is expected to remain for the full global analysis. It is induced by the strongest measurements, HfF^+ and ThO , and according to our parameterization as shown in Tabs. 3 and 4 those two measurements are not affected by any other model parameter. This means the upper-left panel of Fig. 1 factorizes from our global EDM analysis, and we can consider the remaining model parameters separately and without the HfF^+ and ThO measurements.

For the hadronic parameters the situation is different. Again the neutron and Hg measurements are three orders-of-magnitude more constraining than the other measurements. However, as the two model parameters we could as well have chosen $g_\pi^{(0)}$ vs $g_\pi^{(1)}$, without any

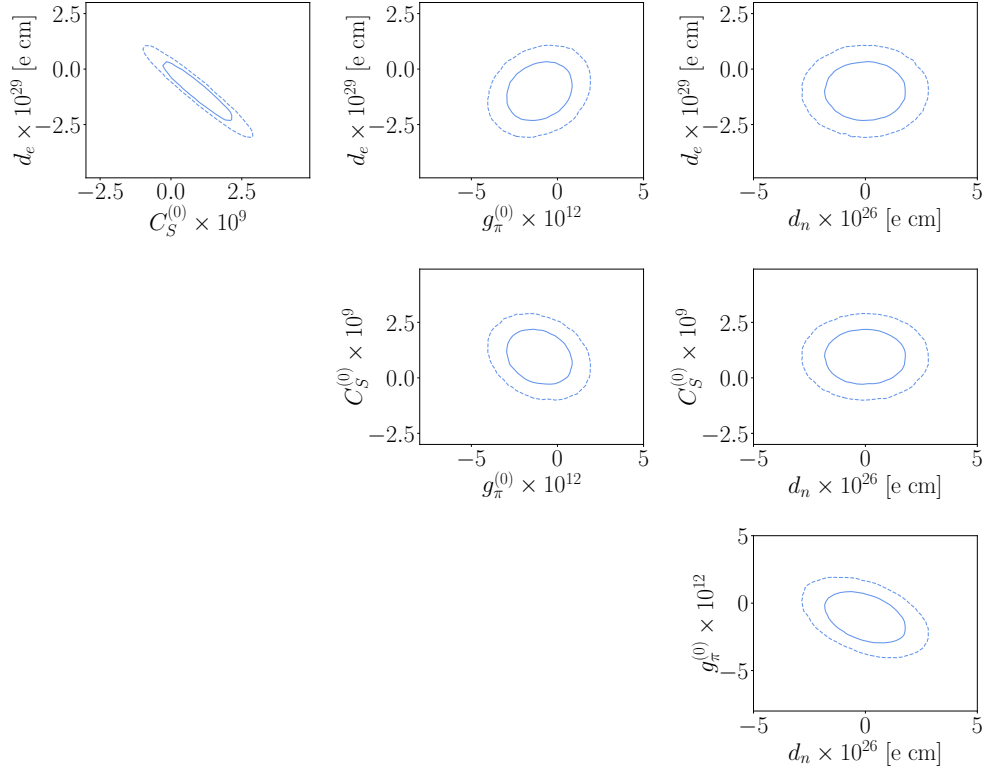


Figure 1: Correlations from the 4-dimensional analysis of $\{d_e, C_S^{(0)}, g_\pi^{(0)}, d_n\}$, based on all EDM measurements but neglecting theory uncertainties. The ellipses indicate 68% and 95% CL.

change in the conclusion. This means that we have to expand the hadronic parameter space next, to see what patterns emerge. The parameters d_e and $C_S^{(0)}$ will be kept factorized for the rest of our global analysis.

To understand the role of approximately flat directions in model space, we can diagonalize and invert the α -matrix given in Tab. 3 for the well-constrained subsystem. To be able to invert the α -matrix, we have to truncate it to a square form. We know that the leading constraints in the $d_e - C_S^{(0)}$ plane come from the ThO and HfF⁺ measurements and can be described by the invertible relation

$$\begin{pmatrix} d_{\text{HfF}^+} \\ d_{\text{ThO}} \end{pmatrix} = \begin{pmatrix} \alpha_{\text{HfF}^+, d_e} & \alpha_{\text{HfF}^+, C_S^{(0)}} \\ \alpha_{\text{ThO}, d_e} & \alpha_{\text{ThO}, C_S^{(0)}} \end{pmatrix} \begin{pmatrix} d_e \\ C_S^{(0)} \end{pmatrix}. \quad (38)$$

We can diagonalize the α -submatrix, find the eigenvalues 1.0 and $5.93 \cdot 10^{-21}$, and invert it to give the model parameters as a function of the measurements,

$$\begin{aligned} \begin{pmatrix} d_e \\ C_S^{(0)} \end{pmatrix} &= \begin{pmatrix} 2.55 & -1.55 \\ -1.69 \cdot 10^{20} & 1.69 \cdot 10^{20} \end{pmatrix} \begin{pmatrix} d_{\text{HfF}^+} \\ d_{\text{ThO}} \end{pmatrix} \\ &= \begin{pmatrix} 2.55 d_{\text{HfF}^+} - 1.55 d_{\text{ThO}} \\ (-1.68 d_{\text{HfF}^+} + 1.69 d_{\text{ThO}}) \cdot 10^{20} \end{pmatrix}. \end{aligned} \quad (39)$$

Approximately flat directions in model space appear because the measurements are uncorrelated. We could determine d_e much more precisely and without any effect from $C_S^{(0)}$ if we could

measure the fully correlated combination $(2.55d_{\text{Hf}^{++}} - 1.55d_{\text{ThO}})$, which is not experimentally realistic. On the other hand, this provides a clear motivation to more carefully consider the role of deliberately-correlated experiments, such as comagnetometer comparisons in which neither EDM can be neglected, within a global context.

Deliberately correlated measurements can be envisioned, for instance via comagnetometry, as already used for the neutron and Xe measurements. In this interpretation it could be advantageous to perform correlated measurements of two systems, with comparable sensitivity to both system EDMs; unlike the usual comagnetometer implementation, where it is usually assumed that one can be neglected entirely.

4.3 Hadronic parameters from closed-shell systems

We define a second restricted model parameter space, for the purely hadronic sector:

$$\{g_{\pi}^{(0)}, g_{\pi}^{(1)}, d_n\}. \quad (40)$$

All three parameters are constrained by the neutron and closed-shell EDMs, while we know from the above discussion that the constraints from closed-shell systems on d_e and $C_S^{(0)}$ are weaker than those from their open-shell counterparts.

From Tab. 4 we see that the neutron and and Hg measurements strongly constrain two of the three hadronic model parameters in Eq.(40). To understand the correlation structure, we show the correlated constraints of the six possible remaining pairs of closed-shell measurements on the three different two-dimensional subspaces of Eq.(40).

Starting with the left panel of Fig. 2, the different pairs of measurements constrain the $g_{\pi}^{(0)}$ vs. $g_{\pi}^{(1)}$ plane with different correlation patterns, implying that a global analysis will constrain the 3-dimensional hadronic subspace much better than any single pair of measurements. In the center panel, the situation changes when we look at the correlations with the neutron EDM d_n . Three combinations are aligned to similar negative correlations between d_n and $g_{\pi}^{(0)}$. In the right panel, the situation is similar for $g_{\pi}^{(1)}$, with a positive correlation and less striking. In both cases the exception are the combinations of Xe respectively with Ra, TlF, and Yb, which constrain d_n extremely well and without any correlation with $g_{\pi}^{(0,1)}$. While this may sound like an advantage, we observe from Tab. 4 and in Fig. 1 that the corresponding limits on d_n are *three orders of magnitude weaker* than would be expected from including the neutron and and Hg measurements.

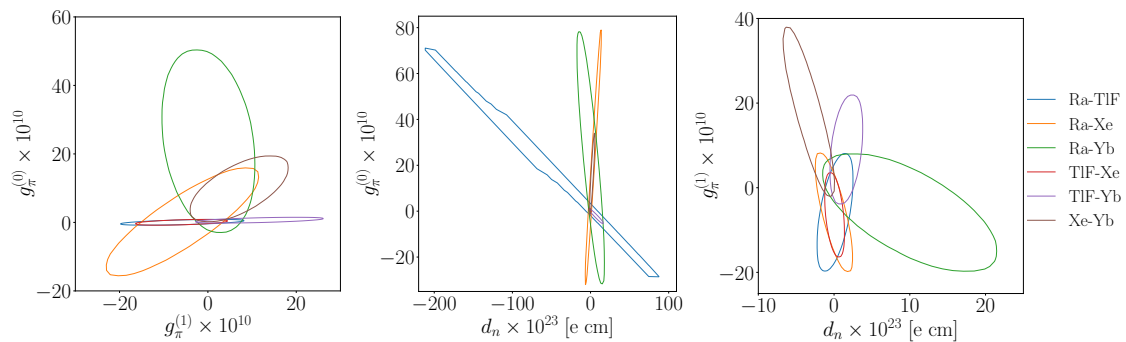


Figure 2: Correlations from three 2-dimensional analyses in the $\{g_{\pi}^{(0)}, g_{\pi}^{(1)}, d_n\}$ parameter space, each based on a different pair of closed-shell EDM measurements, as indicated by the color. The ellipses indicate 68% CL, neglecting theory uncertainties.

Altogether, Fig. 2 confirms that the constraints of the sub-leading four closed-shell measurements on the 3-dimensional hadronic parameter space of Eq.(40) are correlated in a non-trivial manner. Evaluating these correlations requires a global analysis of the, formally, over-constraining set of closed-shell measurements. Inclusion of d_p , C_1 , C_2 , etc. as independent model parameters would further increase the need for complementary experimental constraints.

4.4 Poorly constrained model parameters

Finally, we combine the effects of all remaining parameters,

$$\{C_T^{(0)}, C_P^{(0)}, g_\pi^{(0)}, g_\pi^{(1)}, d_n\}, \quad (41)$$

ignoring the ThO and HfF⁺ measurements, which constrain the factorized $d_e - C_S^{(0)}$ subspace, and also ignoring the neutron and Hg measurements. The latter do constrain the above parameters, but because they are much stronger than all other measurements, they will induce narrow correlations in the allowed 5-dimensional parameter space.

Narrow correlations in a higher-dimensional parameter space vanish when we profile the likelihood onto two-dimensional correlations or even single model parameters. As an exam-

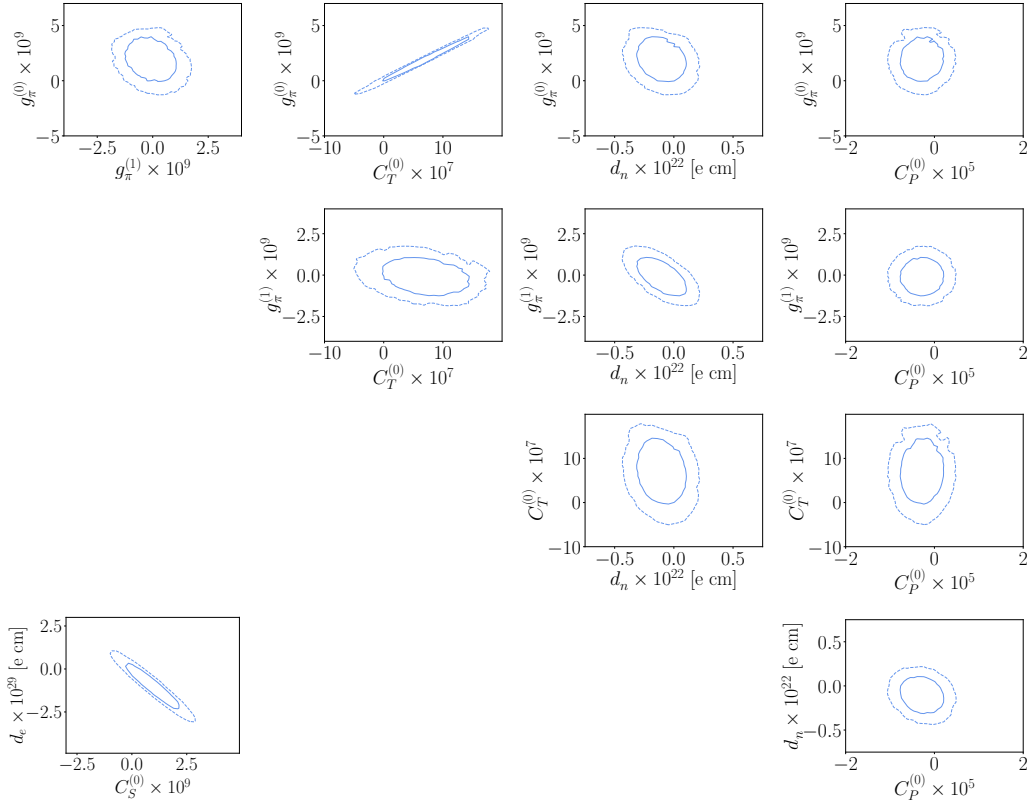


Figure 3: Correlations from the 5-dimensional analysis of $\{C_T^{(0)}, C_P^{(0)}, g_\pi^{(0)}, g_\pi^{(1)}, d_n\}$ and the factorized $d_e - C_S^{(0)}$ plane from Fig. 1. We ignore the neutron and Hg measurements, which induce narrow correlation patterns in the 5-dimensional parameters space and do not affect the profiled 2-dimensional correlations. The ellipses indicate 68% and 95% CL, neglecting theory uncertainties.

ple, consider a two-dimensional parameter space constrained by one strong and one weak measurement. The strong measurement leads to a narrow correlation between the two parameters. When we extract the profile likelihood for one model parameter we can adjust the other model parameter such that the two parameters trace this narrow correlation. This way, the entire length of the correlation pattern gets projected onto the one-dimensional profile likelihoods. The weaker measurement dominates the individual profile likelihoods, while the stronger measurement allows us to link the second model parameter precisely from a value for the first model parameter.

In our case this implies that as long as the correlations from the neutron and Hg measurements cross the entire parameter space, we can ignore these two measurements and their correlation patterns in the following discussion of two-dimensional correlations and single-parameter profile likelihoods. Losing the best few measurements contributing to the global analysis is an unfortunate effect of the conservative profile likelihood approach, but for standard error ellipses it should also exist for Bayesian marginalization. The main difference is that this kind of effect is numerically extremely challenging to compute using marginalization, while it is essentially trivial for the profile likelihood.

Given these considerations, we are left with five model parameters, constrained by seven measurements of comparable constraining power. The only exception we see in Fig. 3 is a strong leading correlation between $g_\pi^{(0)}$ and $C_T^{(0)}$, induced by the fact that for both parameters the TLF measurement is now the strongest by an order of magnitude. All other model parameters are nicely constrained. The allowed range, for instance for $g_\pi^{(0)}$ is of the order 10^{-9} . This can be compared to the constraints from Fig. 1, of the order 10^{-12} . The same hierarchy of measurements can be observed for $g_\pi^{(1)}$ and for d_n , as confirmed by Tab. 4. This means that the 5-dimensional allowed parameter space illustrated by Fig. 3 is crossed by two correlation patterns, roughly three orders of magnitude more narrow than the full parameter space. We emphasize that explaining this extremely narrow correlation poses a fine-tuning problem in model parameter space, which the profile likelihood does not address.

As before, we can truncate the number of available measurements for the poorly constrained 5-dimensional subspace given in Eq.(41), and invert the corresponding α -submatrix to find

$$\begin{pmatrix} C_T^{(0)} \\ C_P^{(0)} \\ g_\pi^{(0)} \\ g_\pi^{(1)} \\ d_n \end{pmatrix} = \begin{pmatrix} 7.14 \cdot 10^{18} & -3.21 \cdot 10^{18} & 6.50 \cdot 10^{19} & -8.77 \cdot 10^{13} & -1.94 \cdot 10^{15} \\ -1.03 \cdot 10^{17} & -5.40 \cdot 10^{19} & 1.09 \cdot 10^{21} & -3.74 \cdot 10^{14} & -3.26 \cdot 10^{16} \\ -2.49 \cdot 10^{14} & -1.45 \cdot 10^{17} & 2.83 \cdot 10^{18} & -2.37 \cdot 10^{12} & -8.60 \cdot 10^{13} \\ 3.10 \cdot 10^{14} & -3.46 \cdot 10^{16} & -2.56 \cdot 10^{18} & 1.58 \cdot 10^{12} & 5.49 \cdot 10^{13} \\ 0. & 0. & 0. & 0. & 1. \end{pmatrix} \begin{pmatrix} d_{\text{TI}} \\ d_{\text{Hg}} \\ d_{\text{Xe}} \\ d_{\text{TLF}} \\ d_n \end{pmatrix}. \quad (42)$$

4.5 Theory uncertainties

Theory uncertainties always appear when using quantum field theory to predict observables, like EDMs, from Lagrangian parameters. No calculation method is arbitrarily precise, and a variety of systematic errors can affect accuracy. While there is some hope for estimating and controlling uncertainties for small expansion parameters, the uncertainties associated with QCD observables at low energies (whether from lattice calculations or sum-rule estimates) are challenging to quantify. The precision of nuclear physics calculations, and their links to effective quantum field theory, also present difficulties. On the other hand we have to estimate all of these uncertainties, and can only ignore them in cases where it can be shown that they are significantly smaller than the experimental uncertainties of the associated measurements.

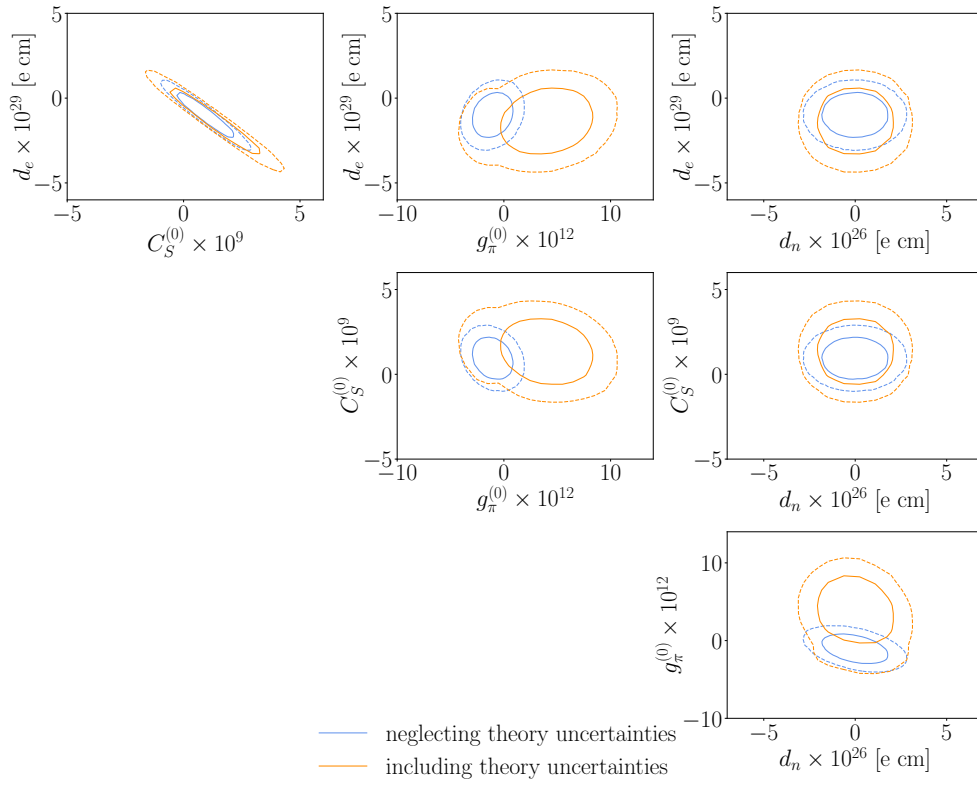


Figure 4: Correlations from the 4-dimensional analysis of $\{d_e, C_S^{(0)}, g_\pi^{(0)}, d_n\}$. The orange curves show the effect of theory uncertainties on the results of Fig. 1. The ellipses indicate 68% and 95% CL.

For our global EDM analysis, theory uncertainties affect the α_{i,c_j} in Eq.(23). The estimated allowable ranges of each coefficient are given in Tab. 3. We include them in SFITTER as uncorrelated theory uncertainties, an assumption that can be modified if necessary. Because of the flat likelihood as a function of the theory nuisance parameter, the profile likelihood approach leads to the theory uncertainties adding linearly, weighted by the respective model parameter. Profiling over independent α -ranges simplifies the numerical evaluation in two ways: first, any parameter–observable pair for which α is compatible with zero will effectively be removed from the global analysis, because the optimal choice of α will remove all contributions from the corresponding model parameter; second, even if we cannot choose α such that measurement and prediction agree, we can choose it to maximize the likelihood and to minimize the impact of the measurement, which means we choose the smallest allowed absolute value of α .

As in Sec. 4.2 we start with the well-constrained 4-dimensional subspace $\{d_e, C_S^{(0)}, g_\pi^{(0)}, d_n\}$. Again, d_e and $C_S^{(0)}$ are constrained by the open-shell molecules HfF^+ and ThO , just as without theory uncertainties. From Tab. 3 we see that we can ignore the theory uncertainty in relating the electron EDM parameter d_e to these systems. In the hadronic sector, the theory uncertainties affecting the relation of $g_\pi^{(0)}$ and d_n to the neutron and Hg EDMs is either trivial or reasonably small, although for the neutron this situation should not be over-interpreted. The quoted uncertainty arises from propagating ranges for the constants within Eq.(27), and not from careful evaluations of the chiral expansion itself.

In Fig. 4 we show the numerical impact of the theory uncertainties on the 2-dimensional correlations. The slightly stronger HfF^+ measurement, which determines the width of the

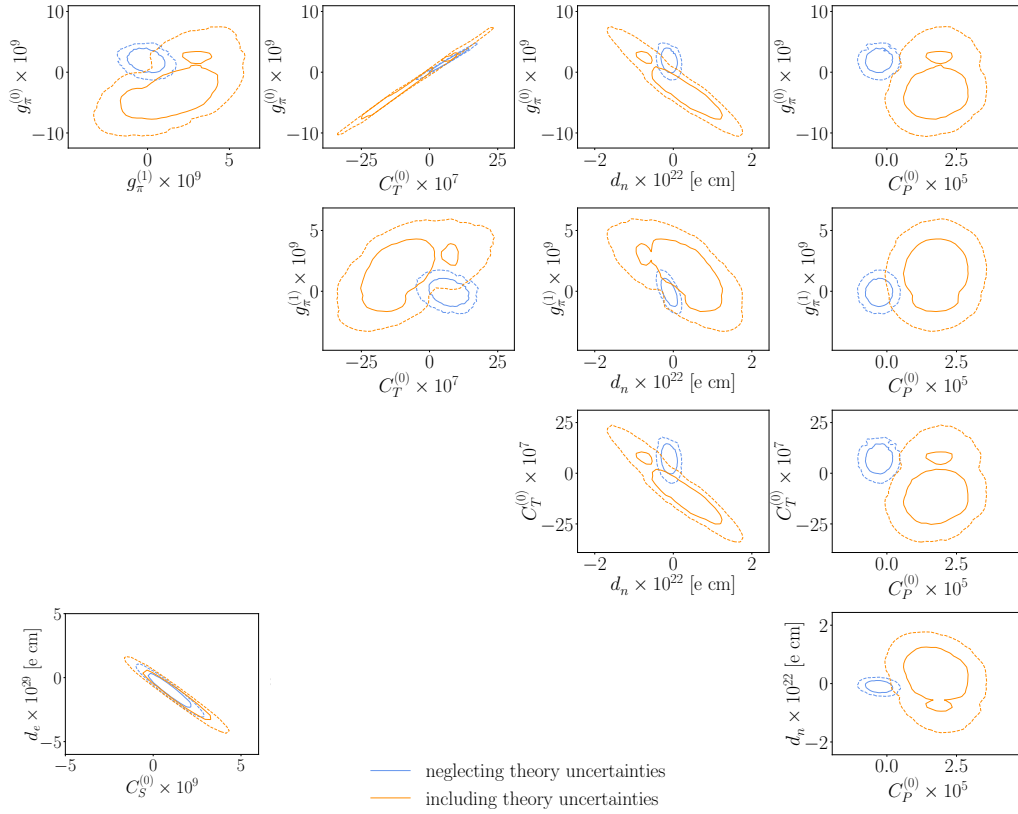


Figure 5: Correlations from the 5-dimensional analysis of $\{C_T^{(0)}, C_P^{(0)}, g_\pi^{(0)}, g_\pi^{(1)}, d_n\}$, and the factorized $d_e - C_S^{(0)}$ plane from Fig. 4. The orange curves show the effect of theory uncertainties on the results of Fig. 3. The ellipses indicate 68% and 95% CL.

correlation pattern, is only minimally affected by the theory uncertainties, while the larger theory uncertainties on the ThO measurement extend the length of the ellipse visibly. The main effect of the theory uncertainties is on $g_\pi^{(0)}$, where they shift the allowed ranges from slightly negative to sizeable positive values. This analysis includes all measurements, so according to Tab. 4 $g_\pi^{(0)}$ is most strongly constrained by the Hg measurement (with a negative central value) and TlF (with a large and positive central value). Adding the theory uncertainties weakens in particular the Hg measurement, which means the two leading constraints get balanced differently, and the entire range moves to the positive values preferred by the TlF measurement.

Moving on, we can now look at the effect of the theory uncertainties on the less-constrained hadronic sector for closed-shell systems, discussed in Sec. 4.3. Here, Tab. 3 shows sizeable, order-one theory uncertainties. In addition, some of the α -values include an allowed zero value when we include theory uncertainties. Specifically, $g_\pi^{(1)}$ is no longer constrained by the Yb measurement and also loses the Hg constraint. In addition some theory uncertainties for closed-shell systems are not consistent with $\alpha = 0$, but are large, which significantly impacts the global analysis.

Finally, we can look at all seven EDM parameters. As for the case without theory uncertainties, the neutron and Hg limits are much more constraining for hadronic parameters than the other measurements. Following the argument given in Sec. 4.4, this means that two-dimensional correlations and single-parameter limits extracted by profiling the likelihoods will not be significantly impacted by these strong measurements. The shift in the constrained two-dimensional correlations are shown in Fig. 5. In comparison their effect on the factorized pa-

parameters d_e and $C_S^{(0)}$ (copied from Fig. 4) is mild, and the constraints on the hadronic model parameters are significantly weaker. The leading correlation in this parameter extraction we found to come from the TLF measurement constraining $g_\pi^{(0)}$ and $C_T^{(0)}$ in a correlated manner. This correlation expands almost to a flat direction when we allow for the additional theory uncertainties. In turn, this large effect extends to the entire space of hadronic parameters, weakening and shifting essentially all constraints. The large shifts addressed in Fig. 5, mostly seen for $C_p^{(0)}$, originate in the treatment and implementation of theory uncertainties. The dominant measurement for $C_p^{(0)}$ suffers from large theory uncertainties, allowing for a shift in estimating the central parameter value, as discussed in Sec. 4.1. This clearly emphasizes the impact of theory uncertainties on the correlations and allowed ranges of the model parameters. To obtain a more coherent picture of these parameter correlations and ranges, theory uncertainties must be reduced (ideally including also a more nuanced treatment of the corresponding likelihoods). There are already some measurements and parameter combinations, like the d_e and $C_S^{(0)}$ subspace, for which theory uncertainties are reasonably well under control (as compared to other elements of Tab. 3). For this case, theory uncertainties produce no significant change of the correlation behavior.

5 Outlook

EDMs are extremely sensitive, targeted probes of one of the most important symmetries of elementary particles, directly related to the observed baryon asymmetry in the Universe. The number of EDM measurements in very different systems has grown rapidly in recent years, leading to the question of how the different measurements can contribute to constraining and understanding CP violation in terms of a fundamental Lagrangian.

We can choose different Lagrangians to answer this question, starting with UV-complete models versus EFTs. In the absence of a specific hint for BSM physics we choose an EFT description. Next, we have a choice of different energy scales with different degrees of freedom. For a first SFITTER analysis we rely on the hadronic-scale Lagrangian, valid at the GeV scale and describing the interactions of electrons and nucleons. After relating the hadronic-scale Lagrangian to its weak-scale SMEFT counterpart we constrain the seven Lagrangian parameters given in Fig. 6 through 11 independent measurements given in Tab. 1.

As a toy analysis we look at single-parameter constraints from individual EDM measurements. These limits are all driven by the same small set of highly constraining measurements, like the open-shell molecular ion HfF^+ , the neutron EDM, or the closed-shell atom Hg. The extremely strong constraints indicated in Fig. 6 do not allow for a cancellation of contributions from two model parameters to a given measurement, at the price of creating a numerical fine-tuning problem in the model parameters. While the single-parameter estimates indicate the strength of an experiment looking for a sign of CP violation, they should not be confused with a measurement of a given parameter.

Our global analysis employs SFITTER, with a focus on the statistical interpretation and a comprehensive uncertainty treatment. First, we ignore all theory uncertainties and only consider experimental uncertainties as uncorrelated and Gaussian (combining the statistical and systematic uncertainties reported in the respective papers). In this case Bayesian marginalization and profile likelihood give the same result.

In Sec. 4.2 we find that a small set of powerful measurements constrains the electron-hadron interactions as well as a subset of the hadronic sector. The correlated limits on the

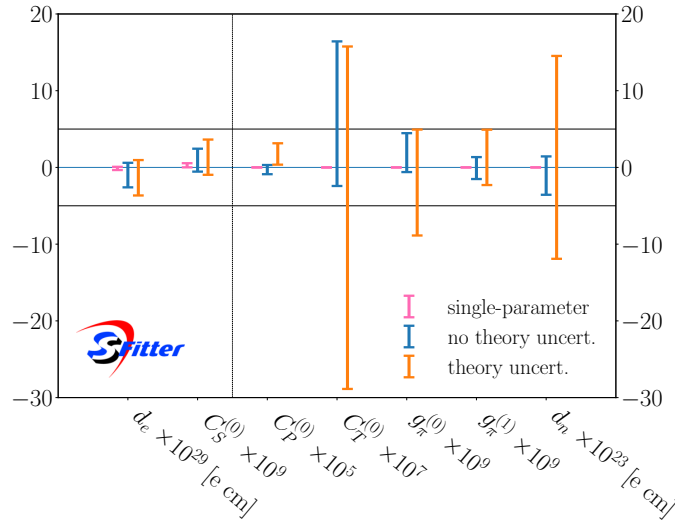


Figure 6: 68% CL constraints from the global EDM analysis on the parameters of the hadronic-scale Lagrangian. We show (i) hugely over-constrained single-parameter ranges allowed by the best available measurement; (ii) over-optimistic allowed ranges for profiled single parameters, ignoring theory uncertainties; (iii) allowed ranges for profiled single parameters including experimental and theory uncertainties.

electron EDM parameter d_e and the scalar coupling $C_S^{(0)}$ are especially strong and factorize from the hadronic sector. Next, we find in Sec. 4.3 that the constraints on the hadronic sector from the closed-shell systems show rich correlations, motivating our global analysis described in Sec. 4.4. For the hadronic parameters, the narrow correlations from the strong neutron and Hg constraints do not appear in profiled 2-dimensional correlations or single-parameter limits. As a result, the hadronic model parameters are constrained much worse than the single-parameter results suggest, as can be seen in Fig. 6.

Finally, we show the same limits including theory uncertainties. Such theory uncertainties always appear when we relate measurements to fundamental Lagrangian parameters. We assume a flat likelihood within allowed ranges of the factors relating the Lagrangian parameters to the EDM predictions. While the impact of the theory uncertainties on the factorized $\{d_e, C_S^{(0)}\}$ sector is relatively mild, the correlated analysis of the hadronic parameters leads to a significant weakening of the constraints on all model parameters.

Acknowledgments

We gratefully acknowledge extremely helpful discussions and correspondence with Robert Berger, Tim Chupp, Vincenzo Cirigliano, Jordy de Vries, Yohei Ema, Victor Flambaum, Timo Fleig, Konstantin Gaul, Maxim Pospelov, and Adam Ritz. We also thank Duarte Azevedo for contributions at an early phase of this project. We thank the ECT* in Trento and EURO-LABS (which received funding from the European Union’s Horizon Europe Research and Innovation programme under grant agreement No 101057511) for support and hospitality while submitting this work and presenting the results for the first time.

NE is funded by the Heidelberg IMPRS *Precision Tests of Fundamental Symmetries*. This research is supported by the Deutsche Forschungsgemeinschaft (DFG, German Research Foundation) under grant 396021762 – TRR 257: *Particle Physics Phenomenology after the Higgs*

Discovery and through Germany's Excellence Strategy EXC 2181/1 – 390900948 (the Heidelberg STRUCTURES Excellence Cluster). Furthermore, we acknowledge support by the state of Baden-Württemberg through bwHPC and the German Research Foundation (DFG) through grant no INST 39/963-1 FUGG (bwForCluster NEMO).

A Alternative parametrization: short-range nucleon EDMs

In an alternative parametrization, we choose $d_{n,p}^{\text{sr}}$ as our model parameters and perform the global SFitter analysis for the set

$$c_j \in \left\{ d_e, C_S^{(0)}, C_T^{(0)}, C_P^{(0)}, g_\pi^{(0)}, g_\pi^{(1)}, d_n^{\text{sr}} \right\}, \quad (43)$$

rather than Eq.(22). To remove the proton EDM parameter we now identify

$$d_p^{\text{sr}} \approx -d_n^{\text{sr}} \quad (44)$$

instead of Eq.(21). We now employ the third line of Eq.(35), dropping $g_\pi^{(2)}$ as before, and noting that the coefficients $\tilde{a}_{i,0}$ and $\tilde{a}_{i,1}$ now include additional terms from the relation connecting $d_{n,p}$ and $d_{n,p}^{\text{sr}}$.

In this appendix we collect the correspondingly adapted versions of all tables and figures from the main body of the paper, derived using this alternative model parameter choice. This alternative parameterization comes with different central values and theory uncertainties for $g_\pi^{(0,1)}$ and $d_{n,p}^{\text{sr}}$. Thus, instead of, for example, $\alpha_{i,g_\pi^{(1)}}$ of the Yb measurement, $\alpha_{i,g_\pi^{(0)}}$ of Xe now includes the zero value and has no impact in the global analysis.

Table 5 provides the hadronic background to the input of our global analysis, given in Tabs. 3 and 6. In some cases, where the valence nucleon is n (respectively p) literature values are not available for the $s_{i,p}$ (respectively, $s_{i,n}$), we given an estimate based on the spin fractions of Tab. 2, as done previously for near-spherical nuclei within the shell model [121]. For some discussion of these estimations, and in particular difficulties associated with $s_{\text{Tl},p}$ and $s_{\text{Hg},n}$ see Ref. [116] and references therein. We do not report the coefficient $s_{\text{Cs},p}$ separately from $\alpha_{\text{Cs},p}$, since the latter includes also contributions from a nuclear magnetic quadrupole moment [56, 122]. This should be borne in mind if using Eq.(35) for ^{133}Cs or nuclei with spin $I > 1/2$; see also [83, 106] for relating a magnetic quadrupole moment to our coefficients $a_{i,j}$. References given for $a_{i,2}$ indicate the sources for central values for all three coefficients $a_{i,j}$; the ranges are inferred from the broader distribution of literature values, see e.g. [14] for a related discussion.

System i	$k_{i,S} [\text{cm}/\text{fm}^3]$	$s_{i,n} [\text{fm}^2]$	$s_{i,p} [\text{fm}^2]$
Tl	$-4.2^{+2.1}_{-1.8} \cdot 10^{-18}$ [35]	$0.14^{\pm 0.03}$	$-0.38^{+1.38}_{-0.45}$
Cs	$-9.99^{+2.9}_{-4.1} \cdot 10^{-18}$ [35]		$0.1^{\pm 0.1}$
^{199}Hg	$-2.26^{\pm 0.23} \cdot 10^{-17}$ [115]	$0.6^{+1.33}_{-0.12}$	$0.06^{+0.20}_{-0.01}$
^{129}Xe	$3.62^{\pm 0.25} \cdot 10^{-18}$ [115]	$0.63^{+0.16}_{-0.12}$	$0.14^{\pm 0.03}$
^{171}Yb	$-2.10^{+0.22}_{-0.0} \cdot 10^{-17}$ [66, 116]	$0.54^{+0.13}_{-0.11}$	$0.054^{+0.016}_{-0.014}$
^{225}Ra	$-8.5^{+0.25}_{-0.3} \cdot 10^{-17}$ [18, 66, 116]	$0.63^{+0.16}_{-0.12}$	$0.14^{+0.04}_{-0.03}$
TlF	$-4.59^{\pm 0.41} \cdot 10^{-13}$ [115]	$0.14^{\pm 0.03}$	$-0.38^{+1.38}_{-0.45}$
	$a_{i,0} [e \text{ fm}^3]$	$a_{i,1} [e \text{ fm}^3]$	$a_{i,2} [e \text{ fm}^3]$
Tl	$0.113^{+0.017}_{-0.008}$	$-0.004^{+0.0}_{-0.006}$	$-0.226^{+0.044}_{-0.03}$ [117]
Cs	$-0.006^{+0.0}_{-0.074}$	$-0.02^{\pm 0.01}$	$-0.04^{+0.0}_{-0.017}$ [118]
^{199}Hg	$0.01^{+0.4}_{-0.005}$	$0.02^{+0.07}_{-0.05}$	$0.02^{+0.04}_{-0.01}$ [14]
^{129}Xe	$-0.008^{+0.003}_{-0.042}$	$0.006^{+0.044}_{-0.003}$	$-0.009^{+0.004}_{-0.091}$ [118]
^{171}Yb	$0.01^{+0.02}_{-0.0}$	$0.02^{+0.034}_{-0.027}$	$0.02^{+0.04}_{-0.01}$ [119]
^{225}Ra	$-1.5^{+0.5}_{-4.5}$	6^{+18}_{-2}	-4^{+3}_{-11} [120]
TlF	$0.113^{+0.017}_{-0.008}$	$-0.004^{+0.0}_{-0.006}$	$-0.226^{+0.044}_{-0.03}$ [117]

Table 5: Inputs for computing the hadronic coefficients in Tabs. 3 and 6.

System i	α_{i,d_e}	$\alpha_{i,C_S}^{(0)} [e \text{ cm}]$	$\alpha_{i,C_p}^{(0)} [e \text{ cm}]$	$\alpha_{i,C_T}^{(0)} [e \text{ cm}]$	$\alpha_{i,g_\pi}^{(0)} [e \text{ cm}]$	$\alpha_{i,g_\pi}^{(1)} [e \text{ cm}]$	$\alpha_{i,d_n}^{\text{st}}$	$\alpha_{i,d_p}^{\text{st}}$
n	—	—	—	—	$1.38^{+0.02}_{-0.02} \cdot 10^{-14}$	$2.73^{+0.02}_{-0.02} \cdot 10^{-16}$	1	(—)
^{205}Tl	$-558^{+28}_{-28} [88]$	$-6.77^{+0.34}_{-0.34} \cdot 10^{-18}$	$1.4^{+2.5}_{-0.8} \cdot 10^{-19}$	$8.8^{+4.0}_{-1.2} \cdot 10^{-21}$	$-6.74^{+4.85}_{-5.12} \cdot 10^{-18}$	$2.20^{+6.53}_{-1.44} \cdot 10^{-19}$	$-5.75^{+3.59}_{-3.77} \cdot 10^{-6}$	$1.61^{+3.35}_{-7.56} \cdot 10^{-5}$
^{133}Cs	$123^{+4}_{-4} [16, 84]$	$7.80^{+0.2}_{-0.8} \cdot 10^{-19}$	$-1.4^{+0.8}_{-2.2} \cdot 10^{-20}$	$1.7^{+0.4}_{-0.4} \cdot 10^{-20}$	—	—	—	—
^{199}Hg	$11.6^{+10}_{-8} \cdot 10^{-3} [35, 89]$	$-1.26^{+0.7}_{-1.2} \cdot 10^{-21}$	$6.6^{+2.4}_{-0.5} \cdot 10^{-23}$	$-6.4^{+3}_{-3} \cdot 10^{-21}$	$-4.70^{+3.13}_{-3.08} \cdot 10^{-18}$	$-6.13^{+16.7}_{-23.7} \cdot 10^{-18}$	$-1.36^{+0.39}_{-0.57} \cdot 10^{-4}$	$-1.36^{+0.39}_{-0.57} \cdot 10^{-5}$
^{129}Xe	$-8^{+16}_{-8} \cdot 10^{-4} [35, 89]$	$-2.1^{+1.2}_{-2.5} \cdot 10^{-22}$	$1.7^{+0.5}_{-0.4} \cdot 10^{-23}$	$1.24^{+0.78}_{-0.61} \cdot 10^{-21}$	$-1.53^{+3.08}_{-3.08} \cdot 10^{-19}$	$2.98^{+23.7}_{-7.1} \cdot 10^{-19}$	$2.29^{+0.57}_{-0.58} \cdot 10^{-5}$	$4.89^{+3.64}_{-1.25} \cdot 10^{-6}$
^{171}Yb	$1.44^{+165}_{-4.5} \cdot 10^{-3} [35]$	$-1.31^{+0.35}_{-1.05} \cdot 10^{-21}$	$4.93^{+3.54}_{-1.55} \cdot 10^{-23}$	$-3.68^{+1.86}_{-2.43} \cdot 10^{-21}$	$-4.21^{+0.94}_{-6.52} \cdot 10^{-18}$	$-5.70^{+7.77}_{-10.4} \cdot 10^{-18}$	$-1.13^{+0.32}_{-0.28} \cdot 10^{-4}$	$-1.13^{+0.32}_{-0.28} \cdot 10^{-5}$
^{225}Ra	$-5.4^{+134}_{-2.0} \cdot 10^{-2} [35]$	$1.13^{+2.94}_{-0.53} \cdot 10^{-20}$	$-7.63^{+2.05}_{-3.88} \cdot 10^{-22}$	$-4.5^{+2.0}_{-0.5} \cdot 10^{-20}$	$1.72^{+5.73}_{-9.67} \cdot 10^{-15}$	$-6.89^{+2.66}_{-2.99} \cdot 10^{-15}$	$-5.38^{+1.20}_{-1.58} \cdot 10^{-4}$	$-1.19^{+0.27}_{-0.35} \cdot 10^{-4}$
TlF	$1.36^{+0.36}_{-0.32} \cdot 10^3 [35]$	$1.44^{+0.3}_{-0.5} \cdot 10^{-16}$	$1.51^{+2.2}_{-3.6} \cdot 10^{-18}$	$1.87^{+0.45}_{-0.17} \cdot 10^{-15}$	$-7.36^{+0.71}_{-2.60} \cdot 10^{-13}$	$2.40^{+0.39}_{-0.53} \cdot 10^{-14}$	$-6.28^{+1.58}_{-1.72} \cdot 10^{-1}$	$1.76^{+2.41}_{-6.76}$
HfF ⁺	1	$9.17^{+0.06}_{-0.06} \cdot 10^{-21}$	—	—	—	—	—	—
ThO	1	$1.51^{+0}_{-0.2} \cdot 10^{-20}$	—	—	—	—	—	—
YbF	1	$8.99^{+0.70}_{-0.70} \cdot 10^{-21}$	—	—	—	—	—	—
	$\eta_{i,d_e}^{(m)} \left[\frac{\text{mrad}}{\text{s e cm}} \right]$	$k_{i,C_S}^{(m)} \left[\frac{\text{mrad}}{\text{s}} \right]$	α_{i,C_p}	α_{i,C_T}	$\alpha_{i,g_\pi}^{(0)}$	$\alpha_{i,g_\pi}^{(1)}$	$\alpha_{i,d_n}^{\text{st}}$	$\alpha_{i,d_p}^{\text{st}}$
HfF ⁺	$3.49^{+0.14}_{-0.14} \cdot 10^{28} [84, 90-93]$	$3.2^{+0.1}_{-0.2} \cdot 10^8 [84, 90, 91]$	—	—	—	—	—	—
ThO	$-1.21^{+0.05}_{-0.39} \cdot 10^{29} [84, 94-96]^{\dagger}$	$-1.82^{+0.42}_{-0.27} \cdot 10^9 [84, 94, 96-98]^{\dagger}$	—	—	—	—	—	—
YbF	$-1.96^{+0.15}_{-0.15} \cdot 10^{28} [84, 97-100]$	$-1.76^{+0.2}_{-0.2} \cdot 10^8 [84, 97-99]$	—	—	—	—	—	—

Table 6: Central values and theory uncertainties for the α -parameters defined in Eq.(23), now using Eq.(27) to treat $d_{n,p}^{\text{st}}$ as model parameters and assuming $d_n^{\text{st}} = -d_p^{\text{st}}$ in lieu of Eq.(21). The coefficients $\alpha_{i,g_\pi}^{(0,1)}$ are accordingly modified via Eq.(35), and differ from those in Tab.3. Here a “—” means that we neglect the dependence in our global analysis. [†]There appears to be an overall sign error in the coefficients reported for ThO in Table 4 of Ref. [84]. The values for Tl and Cs of $\alpha_{i,C_T}^{(0)}$ are estimated by simple analytical calculations [83], and the uncertainties quoted here are estimated as approximately twice those arising from the relevant hadronic matrix elements.

System i	$d_e [e \text{ cm}]$	$C_S^{(0)}$	$C_P^{(0)}$	$C_T^{(0)}$
Tl	$(7.2 \pm 7.7) \cdot 10^{-28}$	$(5.9 \pm 6.4) \cdot 10^{-8}$	$(-2.9 \pm 3.1) \cdot 10^{-6}$	$(-4.5 \pm 4.9) \cdot 10^{-5}$
Cs	$(-1.5 \pm 5.6) \cdot 10^{-26}$	$(-2.3 \pm 8.9) \cdot 10^{-6}$	$(1.3 \pm 5.0) \cdot 10^{-4}$	$(-1.1 \pm 4.1) \cdot 10^{-4}$
^{199}Hg	$(1.9 \pm 2.7) \cdot 10^{-28}$	$(-1.7 \pm 2.5) \cdot 10^{-9}$	$(3.3 \pm 4.7) \cdot 10^{-8}$	$(-3.4 \pm 4.9) \cdot 10^{-10}$
^{129}Xe	$(2.2 \pm 2.3) \cdot 10^{-25}$	$(8.4 \pm 8.7) \cdot 10^{-7}$	$(-1.0 \pm 1.1) \cdot 10^{-5}$	$(-1.4 \pm 1.5) \cdot 10^{-7}$
^{171}Yb	$(-4.7 \pm 3.6) \cdot 10^{-24}$	$(5.2 \pm 4.0) \cdot 10^{-6}$	$(-1.4 \pm 1.1) \cdot 10^{-4}$	$(1.8 \pm 1.4) \cdot 10^{-6}$
^{225}Ra	$(-0.7 \pm 1.1) \cdot 10^{-22}$	$(3.5 \pm 5.3) \cdot 10^{-4}$	$(-5.2 \pm 7.9) \cdot 10^{-3}$	$(-0.9 \pm 1.3) \cdot 10^{-4}$
TlF	$(-1.3 \pm 2.1) \cdot 10^{-26}$	$(-1.2 \pm 2.0) \cdot 10^{-7}$	$(-1.1 \pm 1.9) \cdot 10^{-5}$	$(-0.9 \pm 1.6) \cdot 10^{-8}$
HfF ⁺	$(-1.3 \pm 2.1) \cdot 10^{-30}$	$(-1.4 \pm 2.3) \cdot 10^{-10}$		
ThO	$(4.3 \pm 4.0) \cdot 10^{-30}$	$(2.8 \pm 2.7) \cdot 10^{-10}$		
YbF	$(-2.4 \pm 5.9) \cdot 10^{-28}$	$(-2.7 \pm 6.6) \cdot 10^{-8}$		
	$g_\pi^{(0)}$	$g_\pi^{(1)}$	d_n^{sr}	d_p^{sr}
n	$(0 \pm 8.1) \cdot 10^{-13}$	$(0 \pm 4.1) \cdot 10^{-11}$	$(0 \pm 1.1) \cdot 10^{-26}$	$(0 \pm 1.1) \cdot 10^{-26}$
Tl	$(5.9 \pm 6.4) \cdot 10^{-8}$	$(-1.8 \pm 2.0) \cdot 10^{-6}$	$(7.0 \pm 7.5) \cdot 10^{-20}$	$(-2.5 \pm 2.7) \cdot 10^{-20}$
^{199}Hg	$(-4.7 \pm 6.6) \cdot 10^{-13}$	$(-3.6 \pm 5.1) \cdot 10^{-13}$	$(-1.6 \pm 2.3) \cdot 10^{-26}$	$(-1.6 \pm 2.3) \cdot 10^{-25}$
^{129}Xe	$(1.2 \pm 1.2) \cdot 10^{-9}$	$(5.9 \pm 6.1) \cdot 10^{-10}$	$(-7.7 \pm 7.9) \cdot 10^{-24}$	$(-3.6 \pm 3.7) \cdot 10^{-23}$
^{171}Yb	$(1.6 \pm 1.2) \cdot 10^{-9}$	$(1.2 \pm 0.9) \cdot 10^{-9}$	$(6.0 \pm 4.6) \cdot 10^{-23}$	$(6.0 \pm 4.6) \cdot 10^{-22}$
^{225}Ra	$(2.3 \pm 3.5) \cdot 10^{-9}$	$(-5.8 \pm 8.7) \cdot 10^{-10}$	$(-0.7 \pm 1.1) \cdot 10^{-20}$	$(-3.4 \pm 5.0) \cdot 10^{-20}$
TlF	$(2.3 \pm 3.9) \cdot 10^{-11}$	$(-0.7 \pm 1.2) \cdot 10^{-9}$	$(2.7 \pm 4.6) \cdot 10^{-23}$	$(-1.0 \pm 1.6) \cdot 10^{-23}$

Table 7: Single-parameter ranges allowed by each of the EDM measurements given in Tab. 1, using the coefficients from Tab. 6.

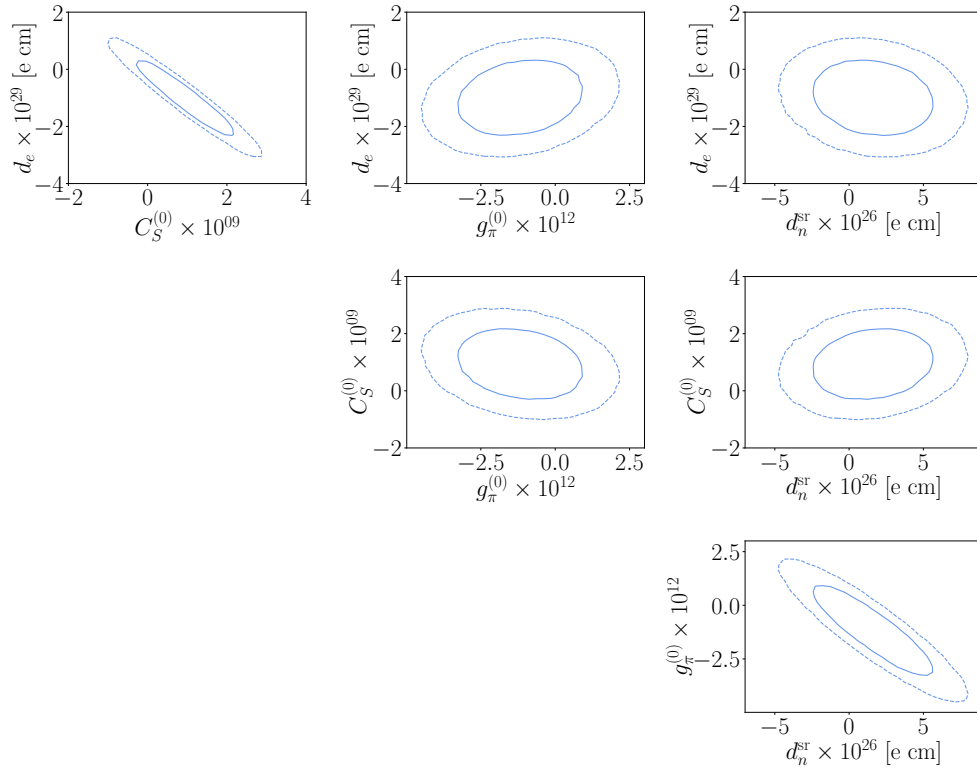


Figure 7: Correlations from the 4-dimensional analysis of $\{d_e, C_S^{(0)}, g_\pi^{(0)}, d_n^{\text{sr}}\}$, based on all EDM measurements but neglecting theory uncertainties. The ellipses indicate 68% and 95% CL. This figure corresponds to Fig. 1 for the $d_{n,p}$ parametrization.

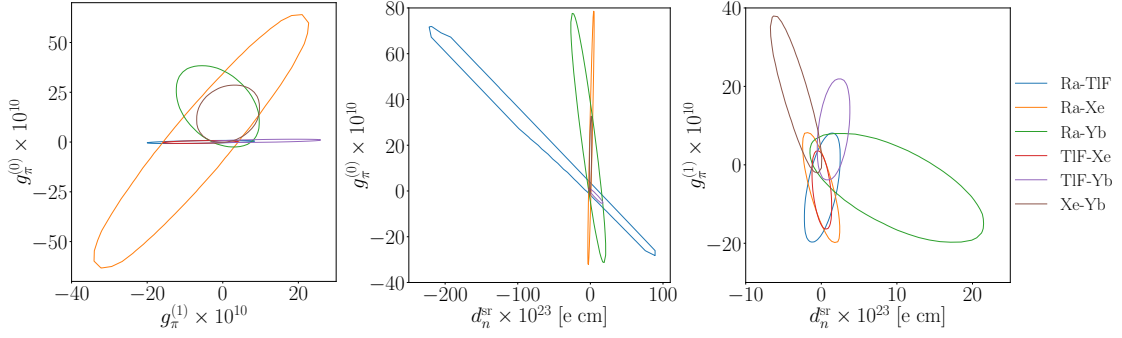


Figure 8: Correlations from three 2-dimensional analyses in the $\{g_\pi^{(0)}, g_\pi^{(1)}, d_n^{sr}\}$ parameter space, each based on a different pair of closed-shell EDM measurements, as indicated by the color. The ellipses indicate 68% CL, neglecting theory uncertainties. This figure corresponds to Fig. 2 for the $d_{n,p}$ parametrization.

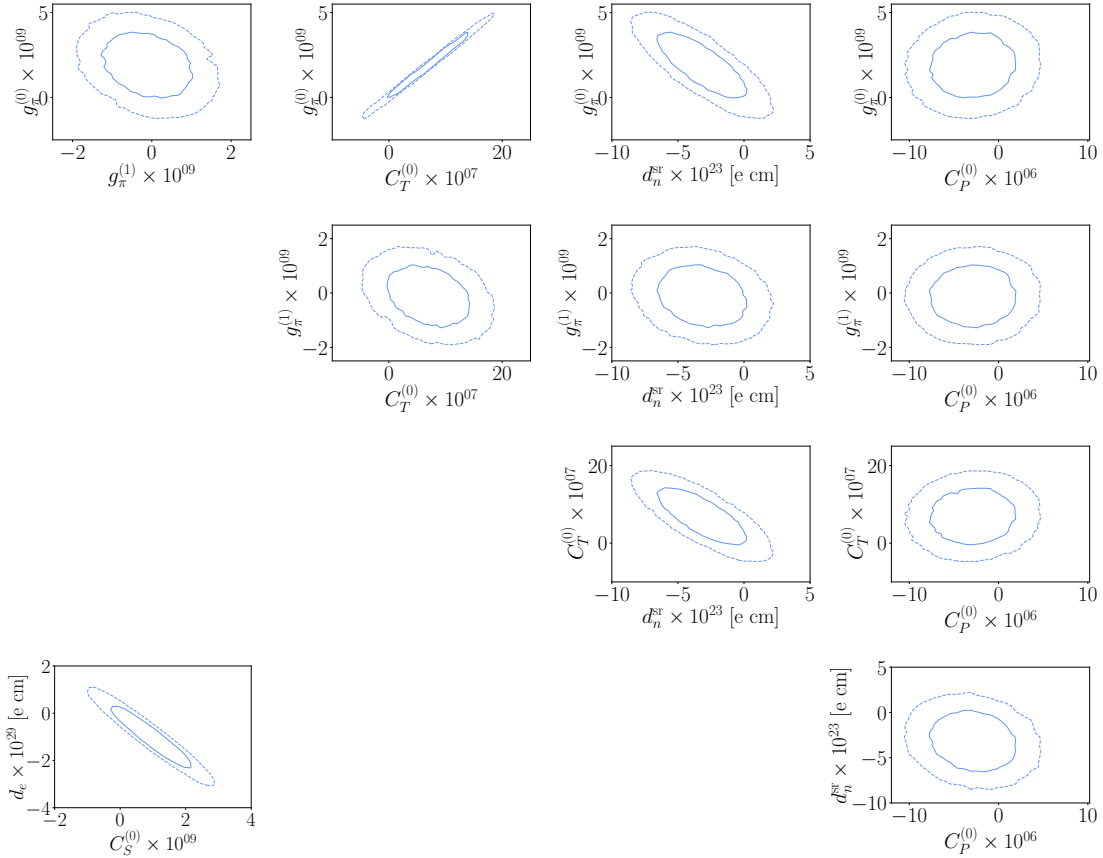


Figure 9: Correlations from the 5-dimensional analysis of $\{C_T^{(0)}, C_P^{(0)}, g_\pi^{(0)}, g_\pi^{(1)}, d_n^{sr}\}$ and the factorized $d_e - C_S^{(0)}$ plane from Fig. 1. We ignore the neutron and Hg measurements, which induce narrow correlation patterns in the 5-dimensional parameters space and do not affect the profiled 2-dimensional correlations. The ellipses indicate 68% and 95% CL, neglecting theory uncertainties. This figure corresponds to Fig. 3 for the $d_{n,p}$ parametrization.

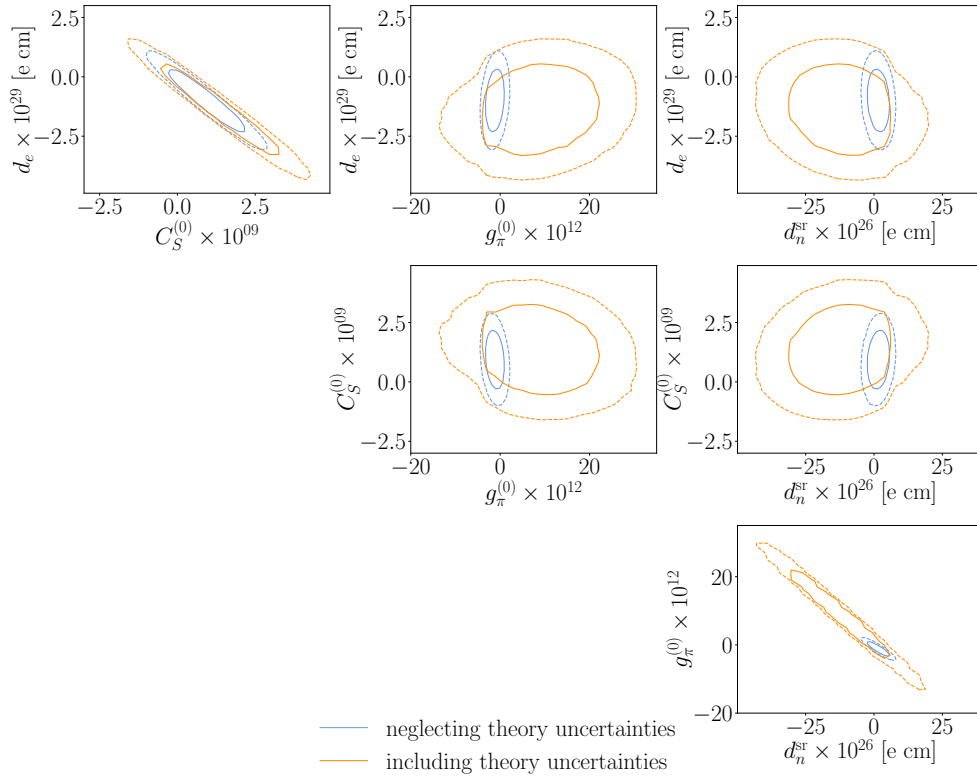


Figure 10: Correlations from the 4-dimensional analysis of $\{d_e, C_S^{(0)}, g_\pi^{(0)}, d_n^{sr}\}$. The orange curves show the effect of theory uncertainties on the results of Fig. 1. The ellipses indicate 68% and 95% CL. This figure corresponds to Fig. 4 for the $d_{n,p}$ parametrization.

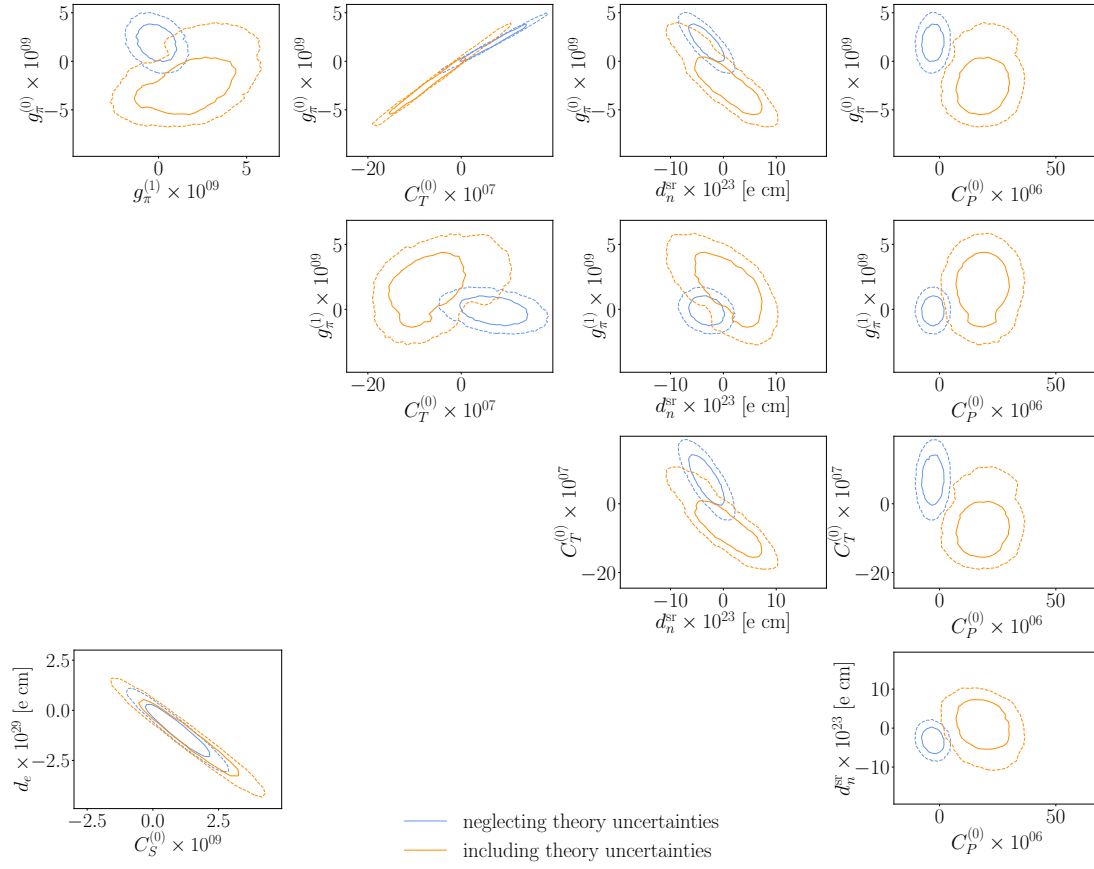


Figure 11: Correlations from the 5-dimensional analysis of $\{C_T^{(0)}, C_P^{(0)}, g_\pi^{(0)}, g_\pi^{(1)}, d_n^{\text{sr}}\}$, and the factorized $d_e - C_S^{(0)}$ plane from Fig. 4. The orange curves show the effect of theory uncertainties on the results of Fig. 3. The ellipses indicate 68% and 95% CL. This figure corresponds to Fig. 5 for the $d_{n,p}$ parametrization.

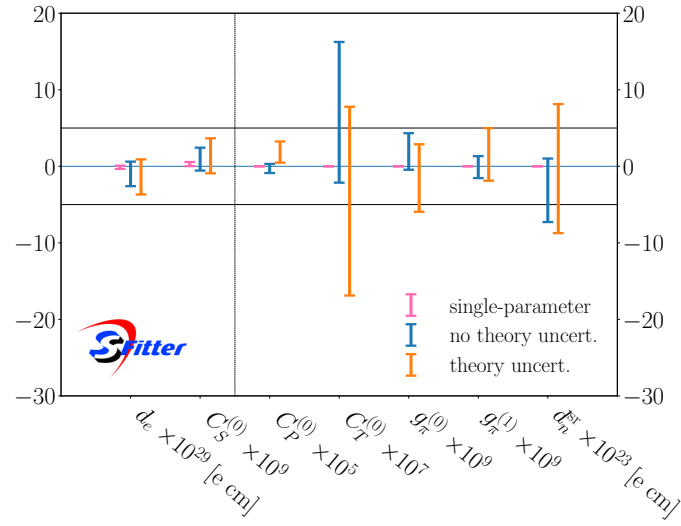


Figure 12: 68% CL constraints from the global EDM analysis on the parameters of the hadronic-scale Lagrangian. We show (i) hugely over-constrained single-parameter ranges allowed by the best available measurement; (ii) over-optimistic allowed ranges for profiled single parameters, ignoring theory uncertainties; (iii) allowed ranges for profiled single parameters including experimental and theory uncertainties. This figure corresponds to Fig. 6 for the $d_{n,p}$ parametrization.

References

- [1] A. D. Sakharov, *Violation of CP Invariance, C asymmetry, and baryon asymmetry of the universe*, [Pisma Zh. Eksp. Teor. Fiz.](#) **5** (1967) 32.
- [2] V. A. Kuzmin, V. A. Rubakov, and M. E. Shaposhnikov, *On the Anomalous Electroweak Baryon Number Nonconservation in the Early Universe*, [Phys. Lett. B](#) **155** (1985) 36.
- [3] M. E. Shaposhnikov, *Baryon Asymmetry of the Universe in Standard Electroweak Theory*, [Nucl. Phys. B](#) **287** (1987) 757.
- [4] A. E. Nelson, D. B. Kaplan, and A. G. Cohen, *Why there is something rather than nothing: Matter from weak interactions*, [Nucl. Phys. B](#) **373** (1992) 453.
- [5] D. E. Morrissey and M. J. Ramsey-Musolf, *Electroweak baryogenesis*, [New J. Phys.](#) **14** (2012) 125003, [arXiv:1206.2942 \[hep-ph\]](#).
- [6] D. Bodeker and W. Buchmüller, *Baryogenesis from the weak scale to the grand unification scale*, [Rev. Mod. Phys.](#) **93** (2021) 3, 035004, [arXiv:2009.07294 \[hep-ph\]](#).
- [7] A. G. Cohen, D. B. Kaplan, and A. E. Nelson, *Progress in electroweak baryogenesis*, [Ann. Rev. Nucl. Part. Sci.](#) **43** (1993) 27, [arXiv:hep-ph/9302210](#).
- [8] M. B. Gavela, P. Hernandez, J. Orloff, and O. Pene, *Standard model CP violation and baryon asymmetry*, [Mod. Phys. Lett. A](#) **9** (1994) 795, [arXiv:hep-ph/9312215](#).
- [9] P. Huet and E. Sather, *Electroweak baryogenesis and standard model CP violation*, [Phys. Rev. D](#) **51** (1995) 379, [arXiv:hep-ph/9404302](#).
- [10] M. B. Gavela, M. Lozano, J. Orloff, and O. Pene, *Standard model CP violation and baryon asymmetry. Part 1: Zero temperature*, [Nucl. Phys. B](#) **430** (1994) 345, [arXiv:hep-ph/9406288](#).
- [11] M. B. Gavela, P. Hernandez, J. Orloff, O. Pene, and C. Quimbay, *Standard model CP violation and baryon asymmetry. Part 2: Finite temperature*, [Nucl. Phys. B](#) **430** (1994) 382, [arXiv:hep-ph/9406289](#).
- [12] A. Riotto and M. Trodden, *Recent progress in baryogenesis*, [Ann. Rev. Nucl. Part. Sci.](#) **49** (1999) 35, [arXiv:hep-ph/9901362](#).
- [13] M. Pospelov and A. Ritz, *Electric dipole moments as probes of new physics*, [Annals Phys.](#) **318** (2005) 119, [arXiv:hep-ph/0504231](#).
- [14] J. Engel, M. J. Ramsey-Musolf, and U. van Kolck, *Electric Dipole Moments of Nucleons, Nuclei, and Atoms: The Standard Model and Beyond*, [Prog. Part. Nucl. Phys.](#) **71** (2013) 21, [arXiv:1303.2371 \[nucl-th\]](#).
- [15] N. Yamanaka, B. K. Sahoo, N. Yoshinaga, T. Sato, K. Asahi, and B. P. Das, *Probing exotic phenomena at the interface of nuclear and particle physics with the electric dipole moments of diamagnetic atoms: A unique window to hadronic and semi-leptonic CP violation*, [Eur. Phys. J. A](#) **53** (2017) 3, 54, [arXiv:1703.01570 \[hep-ph\]](#).
- [16] T. Chupp, P. Fierlinger, M. Ramsey-Musolf, and J. Singh, *Electric dipole moments of atoms, molecules, nuclei, and particles*, [Rev. Mod. Phys.](#) **91** (2019) 1, 015001, [arXiv:1710.02504 \[physics.atom-ph\]](#).

- [17] E. Mereghetti, J. de Vries, W. H. Hockings, C. M. Maekawa, and U. van Kolck, *The Electric Dipole Form Factor of the Nucleon in Chiral Perturbation Theory to Sub-leading Order*, *Phys. Lett. B* **696** (2011) 97, [arXiv:1010.4078 \[hep-ph\]](#).
- [18] T. Chupp and M. Ramsey-Musolf, *Electric Dipole Moments: A Global Analysis*, *Phys. Rev. C* **91** (2015) 3, 035502, [arXiv:1407.1064 \[hep-ph\]](#).
- [19] W. Dekens, J. de Vries, M. Jung, and K. K. Vos, *The phenomenology of electric dipole moments in models of scalar leptoquarks*, *JHEP* **01** (2019) 069, [arXiv:1809.09114 \[hep-ph\]](#).
- [20] D. McKeen, M. Pospelov, and A. Ritz, *Modified Higgs branching ratios versus CP and lepton flavor violation*, *Phys. Rev. D* **86** (2012) 113004, [arXiv:1208.4597 \[hep-ph\]](#).
- [21] S. Dwivedi, D. K. Ghosh, B. Mukhopadhyaya, and A. Shivaji, *Constraints on CP-violating gauge-Higgs operators*, *Phys. Rev. D* **92** (2015) 9, 095015, [arXiv:1505.05844 \[hep-ph\]](#).
- [22] Y. T. Chien, V. Cirigliano, W. Dekens, J. de Vries, and E. Mereghetti, *Direct and indirect constraints on CP-violating Higgs-quark and Higgs-gluon interactions*, *JHEP* **02** (2016) 011, [arXiv:1510.00725 \[hep-ph\]](#).
- [23] V. Cirigliano, W. Dekens, J. de Vries, and E. Mereghetti, *Is there room for CP violation in the top-Higgs sector?*, *Phys. Rev. D* **94** (2016) 1, 016002, [arXiv:1603.03049 \[hep-ph\]](#).
- [24] V. Cirigliano, W. Dekens, J. de Vries, and E. Mereghetti, *Constraining the top-Higgs sector of the Standard Model Effective Field Theory*, *Phys. Rev. D* **94** (2016) 3, 034031, [arXiv:1605.04311 \[hep-ph\]](#).
- [25] S. Inoue, M. J. Ramsey-Musolf, and Y. Zhang, *CP-violating phenomenology of flavor conserving two Higgs doublet models*, *Phys. Rev. D* **89** (2014) 11, 115023, [arXiv:1403.4257 \[hep-ph\]](#).
- [26] D. Fontes, M. Mühlleitner, J. C. Romão, R. Santos, J. a. P. Silva, and J. Wittbrodt, *The C2HDM revisited*, *JHEP* **02** (2018) 073, [arXiv:1711.09419 \[hep-ph\]](#).
- [27] W. Altmannshofer, S. Gori, N. Hamer, and H. H. Patel, *Electron EDM in the complex two-Higgs doublet model*, *Phys. Rev. D* **102** (2020) 11, 115042, [arXiv:2009.01258 \[hep-ph\]](#).
- [28] M. J. Ramsey-Musolf and J. C. Vasquez, *Left-right symmetry and electric dipole moments. a global analysis*, *Physics Letters B* **815** (2021) 136136.
- [29] V. D. Barger, T. Falk, T. Han, J. Jiang, T. Li, and T. Plehn, *CP violating phases in SUSY, electric dipole moments, and linear colliders*, *Phys. Rev. D* **64** (2001) 056007, [arXiv:hep-ph/0101106](#).
- [30] J. R. Ellis, J. S. Lee, and A. Pilaftsis, *Electric Dipole Moments in the MSSM Reloaded*, *JHEP* **10** (2008) 049, [arXiv:0808.1819 \[hep-ph\]](#).
- [31] Y. Li, S. Profumo, and M. Ramsey-Musolf, *A Comprehensive Analysis of Electric Dipole Moment Constraints on CP-violating Phases in the MSSM*, *JHEP* **08** (2010) 062, [arXiv:1006.1440 \[hep-ph\]](#).
- [32] K. Cheung, T.-J. Hou, J. S. Lee, and E. Senaha, *Higgs Mediated EDMs in the Next-to-MSSM: An Application to Electroweak Baryogenesis*, *Phys. Rev. D* **84** (2011) 015002, [arXiv:1102.5679 \[hep-ph\]](#).

- [33] S. F. King, M. Muhlleitner, R. Nevzorov, and K. Walz, *Exploring the CP-violating NMSSM: EDM Constraints and Phenomenology*, *Nucl. Phys. B* **901** (2015) 526, [arXiv:1508.03255 \[hep-ph\]](#).
- [34] T. N. Dao, D. N. Le, and M. Muhlleitner, *Leptonic anomalous magnetic and electric dipole moments in the CP-violating NMSSM with and without inverse seesaw mechanism*, *Eur. Phys. J. C* **82** (2022) 10, 954, [arXiv:2207.12618 \[hep-ph\]](#).
- [35] K. Gaul and R. Berger, *Global analysis of CP-violation in atoms, molecules and role of medium-heavy systems*, *JHEP* **08** (2024) 100, [arXiv:2312.08858 \[hep-ph\]](#).
- [36] R. Lafaye, T. Plehn, and D. Zerwas, *SFITTER: SUSY parameter analysis at LHC and LC*, [arXiv:hep-ph/0404282](#).
- [37] R. Lafaye, T. Plehn, M. Rauch, and D. Zerwas, *Measuring Supersymmetry*, *Eur. Phys. J. C* **54** (2008) 617, [arXiv:0709.3985 \[hep-ph\]](#).
- [38] R. Lafaye, T. Plehn, M. Rauch, D. Zerwas, and M. Duhrssen, *Measuring the Higgs Sector*, *JHEP* **08** (2009) 009, [arXiv:0904.3866 \[hep-ph\]](#).
- [39] I. Brivio, S. Bruggisser, N. Elmer, E. Geoffray, M. Luchmann, and T. Plehn, *To Profile or To Marginalize – A SMEFT Case Study*, *SciPost Phys.* **16** (2024) 035, [arXiv:2208.08454 \[hep-ph\]](#).
- [40] N. Elmer, M. Madigan, T. Plehn, and N. Schmal, *Staying on Top of SMEFT-Likelihood Analyses*, *SciPost Phys.* **18** (2025) 108, [arXiv:2312.12502 \[hep-ph\]](#).
- [41] A. Ghosh, B. Nachman, T. Plehn, L. Shire, T. M. P. Tait, and D. Whiteson, *Statistical patterns of theory uncertainties*, *SciPost Phys. Core* **6** (2023) 045, [arXiv:2210.15167 \[hep-ph\]](#).
- [42] J. de Vries, E. Mereghetti, R. G. E. Timmermans, and U. van Kolck, *The Effective Chiral Lagrangian From Dimension-Six Parity and Time-Reversal Violation*, *Annals Phys.* **338** (2013) 50, [arXiv:1212.0990 \[hep-ph\]](#).
- [43] C. M. Maekawa, E. Mereghetti, J. de Vries, and U. van Kolck, *The Time-Reversal- and Parity-Violating Nuclear Potential in Chiral Effective Theory*, *Nucl. Phys. A* **872** (2011) 117, [arXiv:1106.6119 \[nucl-th\]](#).
- [44] A. Manohar and H. Georgi, *Chiral Quarks and the Nonrelativistic Quark Model*, *Nucl. Phys. B* **234** (1984) 189.
- [45] J. de Vries, A. Gnech, and S. Shain, *Renormalization of CP-violating nuclear forces*, *Phys. Rev. C* **103** (2021) 1, L012501, [arXiv:2007.04927 \[hep-ph\]](#).
- [46] S. Weinberg, *Nuclear forces from chiral Lagrangians*, *Phys. Lett. B* **251** (1990) 288.
- [47] Y. V. Stadnik and V. V. Flambaum, *Nuclear spin-dependent interactions: Searches for WIMP, Axion and Topological Defect Dark Matter, and Tests of Fundamental Symmetries*, *Eur. Phys. J. C* **75** (2015) 3, 110, [arXiv:1408.2184 \[hep-ph\]](#).
- [48] J. C. Berengut, V. V. Flambaum, and E. M. Kava, *Search for variation of fundamental constants and violations of fundamental symmetries using isotope comparisons*, *Phys. Rev. A* **84** (2011) 042510, [arXiv:1109.1893 \[physics.atom-ph\]](#).
- [49] Flavour Lattice Averaging Group (FLAG), Y. Aoki et al., *FLAG Review 2021*, *Eur. Phys. J. C* **82** (2022) 10, 869, [arXiv:2111.09849 \[hep-lat\]](#).

- [50] HERMES, A. Airapetian *et al.*, *Precise determination of the spin structure function $g(1)$ of the proton, deuteron and neutron*, *Phys. Rev. D* **75** (2007) 012007, [arXiv:hep-ex/0609039](#).
- [51] A. Anselm, V. Bunakov, V. Gudkov, and N. Uraltsev, *On the neutron electric dipole moment in the weinberg cp -violation model*, *Physics Letters B* **152** (1985) 1, 116.
- [52] M. Shifman, A. Vainshtein, and V. Zakharov, *Remarks on higgs-boson interactions with nucleons*, *Physics Letters B* **78** (1978) 4, 443.
- [53] S. M. Barr, *T and P odd electron - nucleon interactions and the electric dipole moments of large atoms*, *Phys. Rev. D* **45** (1992) 4148.
- [54] M. Bauer and T. Plehn, *Yet Another Introduction to Dark Matter: The Particle Physics Approach*, vol. 959 of *Lecture Notes in Physics*. Springer, 2019. [arXiv:1705.01987 \[hep-ph\]](#).
- [55] K. R. Dienes, J. Kumar, B. Thomas, and D. Yaylali, *Overcoming Velocity Suppression in Dark-Matter Direct-Detection Experiments*, *Phys. Rev. D* **90** (2014) 1, 015012, [arXiv:1312.7772 \[hep-ph\]](#).
- [56] I. B. Khriplovich and S. K. Lamoreaux, *CP violation without strangeness: Electric dipole moments of particles, atoms, and molecules*. Springer, 1997.
- [57] J. Engel, *Nuclear Schiff Moments and CP Violation*, [arXiv:2501.02744 \[nucl-th\]](#).
- [58] E. S. Ensberg, *Experimental upper limit for the permanent electric dipole moment of rb^{85} by optical pumping techniques*, *Phys. Rev.* **164** (Dec, 1967) 270.
- [59] E. S. Ensberg, *Experimental upper limit for the permanent electric dipole moment of rb^{85} by optical-pumping techniques*, *Phys. Rev.* **153** (Jan, 1967) 36.
- [60] M. A. Player and P. G. H. Sandars, *An experiment to search for an electric dipole moment in the $3p2$ metastable state of xenon*, *Journal of Physics B: Atomic and Molecular Physics* **3** (dec, 1970) 1620.
- [61] S. Eckel, P. Hamilton, E. Kirilov, H. W. Smith, and D. DeMille, *Search for the electron electric dipole moment using Ω -doublet levels in PbO* , *Phys. Rev. A* **87** (2013) 5, 052130, [arXiv:1303.3075 \[physics.atom-ph\]](#).
- [62] S. Eckel, A. O. Sushkov, and S. K. Lamoreaux, *A limit on the electron electric dipole moment using paramagnetic ferroelectric $\text{Eu}_{0.5}\text{Ba}_{0.5}\text{TiO}_3$* , *Phys. Rev. Lett.* **109** (2012) 193003, [arXiv:1208.4420 \[physics.atom-ph\]](#).
- [63] L. Pondrom, R. Handler, M. Sheaff, P. T. Cox, J. Dworkin, O. E. Overseth, T. Devlin, L. Schachinger, and K. J. Heller, *New Limit on the Electric Dipole Moment of the Λ Hyperon*, *Phys. Rev. D* **23** (1981) 814.
- [64] P. V. Coveney and P. G. H. Sandars, *PARITY AND TIME VIOLATING INTERACTIONS IN THALLIUM FLUORIDE*, *J. Phys. B* **16** (1983) 3727.
- [65] T. Fleig and M. Jung, *\mathcal{P} , \mathcal{T} -odd interactions in atomic ^{129}Xe and phenomenological applications*, *Phys. Rev. A* **103** (2021) 1, 012807, [arXiv:2009.07730 \[hep-ph\]](#).
- [66] V. A. Dzuba, V. V. Flambaum, and S. G. Porsev, *Calculation of PT -odd electric dipole moments for diamagnetic atoms Xe-129 , Yb-171 , Hg-199 , Rn-211 , and Ra-225* , *Phys. Rev. A* **80** (2009) 032120, [arXiv:0906.5437 \[physics.atom-ph\]](#).

- [67] M. G. Kozlov, *New Limit on the Scalar P , T Odd Electron Nucleus Interaction*, [Phys. Lett. A **130** \(1988\) 426](#).
- [68] V. V. Flambaum and I. B. Khriplovich, *New Limits on the Electron Dipole Moment and T Nonconserving Electron - Nucleon Interaction*, *Sov. Phys. JETP* **62** (1985) 872.
- [69] C. Abel *et al.*, *Measurement of the Permanent Electric Dipole Moment of the Neutron*, [Phys. Rev. Lett. **124** \(2020\) 8, 081803](#), [arXiv:2001.11966 \[hep-ex\]](#).
- [70] B. C. Regan, E. D. Commins, C. J. Schmidt, and D. DeMille, *New limit on the electron electric dipole moment*, [Phys. Rev. Lett. **88** \(2002\) 071805](#).
- [71] S. A. Murthy, D. Krause, Z. L. Li, and L. R. Hunter, *New Limits on the Electron Electric Dipole Moment from Cesium*, [Phys. Rev. Lett. **63** \(1989\) 965](#).
- [72] T. S. Roussy *et al.*, *A new bound on the electron's electric dipole moment*, [Science **381** \(2023\) 46](#), [arXiv:2212.11841 \[physics.atom-ph\]](#).
- [73] ACME, V. Andreev *et al.*, *Improved limit on the electric dipole moment of the electron*, [Nature **562** \(2018\) 7727, 355](#).
- [74] J. J. Hudson, D. M. Kara, I. J. Smallman, B. E. Sauer, M. R. Tarbutt, and E. A. Hinds, *Improved measurement of the shape of the electron*, [Nature **473** \(2011\) 493](#).
- [75] B. Graner, Y. Chen, E. G. Lindahl, and B. R. Heckel, *Reduced Limit on the Permanent Electric Dipole Moment of $\text{Hg}199$* , [Phys. Rev. Lett. **116** \(2016\) 16, 161601](#), [arXiv:1601.04339 \[physics.atom-ph\]](#). [Erratum: *Phys.Rev.Lett.* 119, 119901 (2017)].
- [76] B. Graner, Y. Chen, E. G. Lindahl, and B. R. Heckel, *Erratum: Reduced limit on the permanent electric dipole moment of ^{199}Hg [*phys. rev. lett.* 116, 161601 (2016)]*, [Phys. Rev. Lett. **119** \(Sep, 2017\) 119901](#).
- [77] N. Sachdeva *et al.*, *New Limit on the Permanent Electric Dipole Moment of ^{129}Xe using ^3He Comagnetometry and SQUID Detection*, [Phys. Rev. Lett. **123** \(2019\) 14, 143003](#), [arXiv:1902.02864 \[physics.atom-ph\]](#).
- [78] F. Allmendinger, I. Engin, W. Heil, S. Karpuk, H.-J. Krause, B. Niederländer, A. Offenhäusser, M. Repetto, U. Schmidt, and S. Zimmer, *Measurement of the permanent electric dipole moment of the ^{129}Xe atom*, [Phys. Rev. A **100** \(Aug, 2019\) 022505](#).
- [79] T. A. Zheng, Y. A. Yang, S. Z. Wang, J. T. Singh, Z. X. Xiong, T. Xia, and Z. T. Lu, *Measurement of the Electric Dipole Moment of $\text{Yb}171$ Atoms in an Optical Dipole Trap*, [Phys. Rev. Lett. **129** \(2022\) 8, 083001](#), [arXiv:2207.08140 \[physics.atom-ph\]](#).
- [80] M. Bishof *et al.*, *Improved limit on the ^{225}Ra electric dipole moment*, [Phys. Rev. C **94** \(2016\) 2, 025501](#), [arXiv:1606.04931 \[nucl-ex\]](#).
- [81] D. Cho, K. Sangster, and E. A. Hinds, *Search for time reversal symmetry violation in thallium fluoride using a jet source*, [Phys. Rev. A **44** \(1991\) 2783](#).
- [82] T. Fleig and L. V. Skripnikov, *\mathcal{P} , \mathcal{T} -Violating and Magnetic Hyperfine Interactions in Atomic Thallium*, [Symmetry **12** \(2020\) 4, 498](#), [arXiv:1910.11596 \[physics.atom-ph\]](#).
- [83] J. Ginges and V. Flambaum, *Violations of fundamental symmetries in atoms and tests of unification theories of elementary particles*, [Physics Reports **397** \(2004\) 2, 63](#).

- [84] T. Fleig and M. Jung, *Model-independent determinations of the electron EDM and the role of diamagnetic atoms*, *JHEP* **07** (2018) 012, [arXiv:1802.02171 \[hep-ph\]](#).
- [85] T. Fleig, *PT -odd weak neutral current interactions in the TlF molecule*, *Phys. Rev. A* **109** (2024) 2, 022807, [arXiv:2311.06376 \[physics.atom-ph\]](#).
- [86] J. de Vries, P. Draper, K. Fuyuto, J. Kozaczuk, and B. Lillard, *Uncovering an axion mechanism with the EDM portfolio*, *Phys. Rev. D* **104** (2021) 5, 055039, [arXiv:2107.04046 \[hep-ph\]](#).
- [87] Particle Data Group, R. L. Workman and Others, *Review of Particle Physics*, *PTEP* **2022** (2022) 083C01.
- [88] T. Fleig and L. V. Skripnikov, *P , t -violating and magnetic hyperfine interactions in atomic thallium*, *Symmetry* **12** (2020) 4, .
- [89] A.-M. Mårtensson-Pendrill and P. Öster, *Calculations of atomic electric dipole moments*, *Physica Scripta* **36** (sep, 1987) 444.
- [90] L. V. Skripnikov, *Communication: Theoretical study of HfF^+ cation to search for the T , P -odd interactions*, *The Journal of Chemical Physics* **147** (07, 2017) 021101, https://pubs.aip.org/aip/jcp/article-pdf/doi/10.1063/1.4993622/13976956/021101_1_online.pdf.
- [91] T. Fleig, *P , T -odd and magnetic hyperfine-interaction constants and excited-state lifetime for HfF^+* , *Phys. Rev. A* **96** (2017) 4, 040502, [arXiv:1706.02893 \[physics.atom-ph\]](#).
- [92] A. N. Petrov, N. S. Mosyagin, T. A. Isaev, and A. V. Titov, *Theoretical study of HfF^+ in search of the electron electric dipole moment*, *Phys. Rev. A* **76** (2007) 030501, [arXiv:physics/0611254](#).
- [93] E. R. Meyer, J. L. Bohn, and M. P. Deskevich, *Candidate molecular ions for an electron electric dipole moment experiment*, *Phys. Rev. A* **73** (Jun, 2006) 062108.
- [94] L. V. Skripnikov, *Combined 4-component and relativistic pseudopotential study of ThO for the electron electric dipole moment search*, *The Journal of Chemical Physics* **145** (12, 2016) 214301, https://pubs.aip.org/aip/jcp/article-pdf/doi/10.1063/1.4968229/15523128/214301_1_online.pdf.
- [95] E. R. Meyer and J. L. Bohn, *Prospects for an electron electric dipole moment search in metastable ThO and ThF*, *Phys. Rev. A* **78** (2008) 010502, [arXiv:0805.0161 \[physics.atom-ph\]](#).
- [96] M. Denis and T. Fleig, *In search of discrete symmetry violations beyond the standard model: Thorium monoxide reloaded*, *The Journal of Chemical Physics* **145** (12, 2016) 214307, https://pubs.aip.org/aip/jcp/article-pdf/doi/10.1063/1.4968597/15523220/214307_1_online.pdf.
- [97] V. A. Dzuba, V. V. Flambaum, and C. Harabati, *Relations between matrix elements of different weak interactions and interpretation of the parity-nonconserving and electron electric-dipole-moment measurements in atoms and molecules*, *Phys. Rev. A* **84** (Nov, 2011) 052108.
- [98] V. A. Dzuba, V. V. Flambaum, and C. Harabati, *Erratum: Relations between matrix elements of different weak interactions and interpretation of the parity-nonconserving and electron electric-dipole-moment measurements in atoms and molecules [phys. rev. a 84, 052108 (2011)]*, *Phys. Rev. A* **85** (Feb, 2012) 029901.

- [99] A. Sunaga, M. Abe, M. Hada, and B. P. Das, *Relativistic coupled-cluster calculation of the electron-nucleus scalar-pseudoscalar interaction constant W_s in ybf*, [Phys. Rev. A **93** \(Apr, 2016\) 042507](#).
- [100] M. Abe, G. Gopakumar, M. Hada, B. P. Das, H. Tatewaki, and D. Mukherjee, *Application of relativistic coupled-cluster theory to the effective electric field in ybf*, [Phys. Rev. A **90** \(Aug, 2014\) 022501](#).
- [101] Y. Ema, T. Gao, and M. Pospelov, *Improved Indirect Limits on Muon Electric Dipole Moment*, [Phys. Rev. Lett. **128** \(2022\) 13, 131803](#), [arXiv:2108.05398 \[hep-ph\]](#).
- [102] ACME, J. Baron *et al.*, *Methods, Analysis, and the Treatment of Systematic Errors for the Electron Electric Dipole Moment Search in Thorium Monoxide*, [New J. Phys. **19** \(2017\) 7, 073029](#), [arXiv:1612.09318 \[physics.atom-ph\]](#).
- [103] T. Fleig and M. Jung, *\mathcal{P} , \mathcal{T} -odd interactions in atomic ^{129}Xe and phenomenological applications*, [Phys. Rev. A **103** \(Jan, 2021\) 012807](#).
- [104] V. Flambaum and I. Khriplovich, *New bounds on the electric dipole moment of the electron and on t -odd electron-nucleon coupling*, *Zh. Eksp. Theor. Fiz* **89** (1985) 1505.
- [105] L. I. Schiff, *Measurability of Nuclear Electric Dipole Moments*, [Phys. Rev. **132** \(1963\) 2194](#).
- [106] V. V. Flambaum, D. DeMille, and M. G. Kozlov, *Time-reversal symmetry violation in molecules induced by nuclear magnetic quadrupole moments*, [Phys. Rev. Lett. **113** \(2014\) 103003](#), [arXiv:1406.6479 \[physics.atom-ph\]](#).
- [107] K. Yanase and N. Shimizu, *Large-scale shell-model calculations of nuclear Schiff moments of ^{129}Xe and ^{199}Hg* , [Phys. Rev. C **102** \(2020\) 6, 065502](#), [arXiv:2006.15142 \[nucl-th\]](#).
- [108] A. Butter, S. Murgia, T. Plehn, and T. M. P. Tait, *Saving the MSSM from the Galactic Center Excess*, [Phys. Rev. D **96** \(2017\) 3, 035036](#), [arXiv:1612.07115 \[hep-ph\]](#).
- [109] M. Klute, R. Lafaye, T. Plehn, M. Rauch, and D. Zerwas, *Measuring Higgs Couplings from LHC Data*, [Phys. Rev. Lett. **109** \(2012\) 101801](#), [arXiv:1205.2699 \[hep-ph\]](#).
- [110] A. Biekötter, T. Corbett, and T. Plehn, *The Gauge-Higgs Legacy of the LHC Run II*, [SciPost Phys. **6** \(2019\) 6, 064](#), [arXiv:1812.07587 \[hep-ph\]](#).
- [111] I. Brivio, S. Bruggisser, F. Maltoni, R. Moutafis, T. Plehn, E. Vryonidou, S. Westhoff, and C. Zhang, *O new physics, where art thou? A global search in the top sector*, [JHEP **02** \(2020\) 131](#), [arXiv:1910.03606 \[hep-ph\]](#).
- [112] D. López-Val, T. Plehn, and M. Rauch, *Measuring extended Higgs sectors as a consistent free couplings model*, [JHEP **10** \(2013\) 134](#), [arXiv:1308.1979 \[hep-ph\]](#).
- [113] I. Brivio, S. Bruggisser, E. Geoffray, W. Killian, M. Krämer, M. Luchmann, T. Plehn, and B. Summ, *From models to SMEFT and back?*, [SciPost Phys. **12** \(2022\) 1, 036](#), [arXiv:2108.01094 \[hep-ph\]](#).
- [114] A. Hocker, H. Lacker, S. Laplace, and F. Le Diberder, *A New approach to a global fit of the CKM matrix*, [Eur. Phys. J. C **21** \(2001\) 225](#), [arXiv:hep-ph/0104062](#).
- [115] M. Hubert and T. Fleig, *Electric dipole moments generated by nuclear Schiff moment interactions: A reassessment of the atoms $\text{Xe}129$ and $\text{Hg}199$ and the molecule $\text{TlF}205$* , [Phys. Rev. A **106** \(2022\) 2, 022817](#), [arXiv:2203.04618 \[physics.atom-ph\]](#).

- [116] V. V. Flambaum and V. A. Dzuba, *Electric dipole moments of atoms and molecules produced by enhanced nuclear Schiff moments*, [Phys. Rev. A **101** \(2020\) 4, 042504](#), [arXiv:1912.03598 \[physics.atom-ph\]](#).
- [117] V. V. Flambaum, I. B. Khriplovich, and O. P. Sushkov, *On the P and T Nonconserving Nuclear Moments*, [Nucl. Phys. A **449** \(1986\) 750](#).
- [118] V. F. Dmitriev, R. A. Sen'kov, and N. Auerbach, *Effects of core polarization on the nuclear Schiff moment*, [Phys. Rev. C **71** \(2005\) 035501](#), [arXiv:nucl-th/0408065](#).
- [119] V. A. Dzuba, V. V. Flambaum, and J. S. M. Ginges, *Atomic electric dipole moments of He and Yb induced by nuclear Schiff moments*, [Phys. Rev. A **76** \(2007\) 034501](#), [arXiv:0705.4001 \[physics.atom-ph\]](#).
- [120] J. Dobaczewski and J. Engel, *Nuclear time-reversal violation and the Schiff moment of Ra-225*, [Phys. Rev. Lett. **94** \(2005\) 232502](#), [arXiv:nucl-th/0503057](#).
- [121] V. A. Dzuba, V. V. Flambaum, and P. G. Silvestrov, *Bounds on Electric Dipole Moments and T Violating Weak Interactions of the Nucleons*, [Phys. Lett. B **154** \(1985\) 93](#).
- [122] I. B. Khriplovich, *Limit on the Proton Electric Dipole Moment from Atomic Experiments*, [Sov. Phys. JETP **44** \(1976\) 25](#).